

# Reappraisal and new material of the holotype of *Draconyx loureiroi* (Ornithischia: Iguanodontia) provide insights on the *tempo* and *modo* of evolution of thumb-spiked dinosaurs

FILIPPO MARIA ROTATORI<sup>1,2,\*</sup>, MIGUEL MORENO-AZANZA<sup>1,2,3</sup> and OCTÁVIO MATEUS<sup>1,2</sup>

<sup>1</sup>GEOTEC, Department of Earth Sciences, NOVA School of Science and Technology, Campus de Caparica, P-2829 516 Caparica, Portugal

<sup>2</sup>Museu da Lourinhã, Rua João Luis de Moura 95, 2530-158, Lourinhã, Portugal

<sup>3</sup>Grupo Aragosaurus-IUCA, Facultad de Ciencias, Universidad de Zaragoza, 50009, Zaragoza, Spain

Received 9 April 2021; revised 9 November 2021; accepted for publication 26 November 2021

The Upper Jurassic Lourinhã Formation is well known for its rich assemblage of fossil vertebrates. In this formation, ornithopod dinosaurs are represented by two iguanodontian species, *Eousdryosaurus nanohallucis* and *Draconyx loureiroi*. We recently became aware of unreported material belonging to the holotype of *Draconyx loureiroi*, consisting of partially articulated manual elements. We here re-describe the holotype specimen ML 357, including the newly discovered material. The specimen was subjected to CT-scanning and its surface data used to assess anatomical characters. Linear measurements of metatarsal III were used to estimate the body length of the specimen. The *Draconyx loureiroi* holotype was included in two datasets and analysed with maximum parsimony and Bayesian inference approaches to estimate evolutionary rates among Iguanodontia. We present evidence that *Draconyx loureiroi* is a valid taxon nested in Styrcosterna and is clearly diagnosable by a unique combination of characters. Both maximum parsimony and Bayesian inference indicate high evolutionary rates across the Jurassic/Cretaceous transition for the base of Iguanodontia. Length estimation suggests that *Draconyx loureiroi* was a relatively small, bipedal and possibly cursorial animal. Given its basal phyletic position, we interpret this bauplan as the ancestral condition for Styrcosterna, that only later in the Cretaceous evolved into giant quadrupedal forms.

KEYWORDS: Ornithopoda – Phylogenetic analysis – Bayesian inference – Jurassic – Europe.

## INTRODUCTION

Iguanodontia (*sensu* Madzia *et al.*, 2018) is a highly diverse clade of ornithischian dinosaurs with basal (non-hadrosauroid) forms as a frequent component of Late Jurassic and Early Cretaceous ecosystems (Galton, 1980, 2006, 2009; McDonald *et al.*, 2010b; Foster, 2020). Despite their long history of research (Mantell, 1825) and their widespread biogeographic distribution, most of what is known of the anatomy and phyletic relationships of Late Jurassic species is relegated to the North American continent and Africa. Europe has also produced many relevant specimens and species dated to the Early Cretaceous (Norman, 1980, 1986, 2004,

2015; McDonald *et al.*, 2012), while Late Jurassic taxa are represented by fewer and, in some cases, incomplete specimens (Galton & Powell, 1980; Mateus & Antunes, 2001; Ruiz-Omeñaca *et al.*, 2006, Escaso *et al.*, 2014).

The relationships at the base of Iguanodontia (generally within basal Ornithopoda) have undergone several changes in recent years (Boyd, 2015; Dieudonné *et al.*, 2016, 2021; Bell *et al.*, 2018; Madzia *et al.*, 2018; Herne *et al.*, 2019; Rozadilla *et al.*, 2019), profiling a more complex evolutionary history of this clade than previously inferred (e.g. McDonald, 2012; Norman, 2015). After McDonald (2012) and derived matrices (Xu *et al.*, 2018; Verdú *et al.*, 2018, 2019), several studies have considered the global relationships of Iguanodontia, often focusing on less inclusive clades (Boyd, 2015; Madzia *et al.*,

\*Corresponding author. E-mail: [filippo.rotatori.93@gmail.com](mailto:filippo.rotatori.93@gmail.com)

2018; Dieudonné *et al.*, 2021). European taxa, despite their paucity and poor preservation, may help to untangle the intricate evolutionary relationships at the root of Iguanodontia. Recently, two independent lines of evidence (ichnological and body fossil records) have pointed out that the diversity of iguanodontians in the Late Jurassic of Europe may be severely underestimated, suggesting the presence of styracosternans more similar to Early Cretaceous forms than to other coeval iguanodontians (Castanera *et al.*, 2020, 2021; Rotatori *et al.*, 2020).

*Draconyx loureiroi* Mateus & Antunes, 2001 is one of two ornithopod taxa described from the Late Jurassic of the Iberian Peninsula. The holotype ML 357, and the only specimen so far, is a medium-sized iguanodontian that was recovered from the Upper Jurassic Lourinhã Formation (Portugal) in 1991 (Mateus & Antunes, 2001). Histological studies have shown that ML 357 is a senile individual, approximately 30 years old (Waskow & Mateus, 2017). Mateus & Antunes (2001) classified the specimen as a basal iguanodontian, attributing the species to the family ‘Camptosauridae’, composed at that time of the species *Camptosaurus dispar* Marsh, 1879, ‘*Camptosaurus*’ (= *Cumnoria*) *prestwichii* Hulke, 1880, *Callovosaurus leedsi* Ruiz-Omeñaca *et al.* 2006 and *Draconyx loureiroi*. Subsequent analyses by McDonald (2011) recovered the genus *Camptosaurus* as paraphyletic, while Ruiz-Omeñaca *et al.* (2006) have recovered *Callovosaurus leedsi* as a member of Dryosauridae. Since then, the clade ‘Camptosauridae’ has been recovered from a few analyses with weak support (i.e. Verdú *et al.*, 2018). Other authors treated *Draconyx loureiroi* as a wildcard taxon (McDonald, 2012) or they excluded it a priori in their analyses due to its fragmentary nature. Recently, Verdú *et al.* (2018) recovered *D. loureiroi* in a more derived position than *Camptosaurus dispar*.

In the present study, we contribute to our knowledge of the anatomy and phylogenetic relationships of Late Jurassic European ornithopod taxa by re-describing the holotype of *Draconyx loureiroi* (ML 357) and including undescribed material that was made available by the original collector. We analyse in detail its phylogenetic relationships and its significance for the evolutionary history of iguanodontians via time-calibrated analyse, employing both maximum parsimony and Bayesian inference. The results indicate a more deeply nested position in Ankylopollexia than previously inferred by other authors.

**Abbreviations:** ML, Museu da Lourinhã, Lourinhã, Portugal; SHN, Sociedade de História Natural, Torres Vedras, Portugal; NMNH, National Museum of Natural History, Washington DC, USA.

## GEOLOGICAL SETTING

The Lourinhã Formation (Fig. 1) is a heterogeneous siliciclastic succession of continental deposits dated to the Kimmeridgian–Tithonian interval and located in the Meso-Cenozoic Lusitanian Basin (Kullberg *et al.*, 2014), in which subdivisions have been debated (Hill, 1989; Taylor *et al.*, 2014). Generally, it is composed of sandstones and mudstones with rare limestone intercalations, representing a braided fluvial system and alluvial fans, with occasional marine transgressions (Hill, 1989; Taylor *et al.*, 2014). Since a detailed revision and overview of this lithostratigraphic unit is beyond the scope of the current study, for simplicity the subdivisions described by Mateus *et al.* (2017) are used. The Lourinhã Fm. outcrops in two sub-basins: the Consolação and Turcifal. In the first, three members are distinctly recognizable (from bottom to top): Porto Novo/Praia da Amoreira Member, Praia Azul Member and the Santa Rita Member. In the Turcifal sub-basin, the only member outcropping is the Assenta Member, which is laterally equivalent to the Santa Rita Member.

The *Draconyx loureiroi* holotype was recovered from the Praia Azul Member, which is composed of three extensive carbonated shell-layers, cutting a succession of fine mudstones (Hill, 1989; Taylor *et al.*, 2014). Each layer represents a marine transgression episode along the second layer in the transition between the Kimmeridgian and Tithonian stages (Hill, 1989; Taylor *et al.*, 2014; Mateus *et al.*, 2017). The specimen ML 357 was recovered just above the second layer and is, therefore, considered lowermost Tithonian in age (Mateus & Antunes, 2001).

## MATERIAL AND METHODS

ML 357 is a partial skeleton, including appendicular and axial elements. It was recovered in 1991 and has been housed in the collections of the Museu da Lourinhã since. The specimen includes an almost complete and articulated foot and several other disarticulated and isolated postcranial elements. We were recently informed by the discoverer of this specimen, Carlos Anunciação, of the existence of unreported material belonging to the holotype specimen, stored in his home since its collection in 1991. This unreported material has now been donated to the Museu da Lourinhã and is added to the original ML 357 entry number. This newly donated material includes manual phalanges and further carpal elements. It is clearly from the same locality, matches in size and is consistent in other features of ML 357. Furthermore, the lack of repeated elements supports the interpretation that both the old and the new material represent the same individual. In addition,

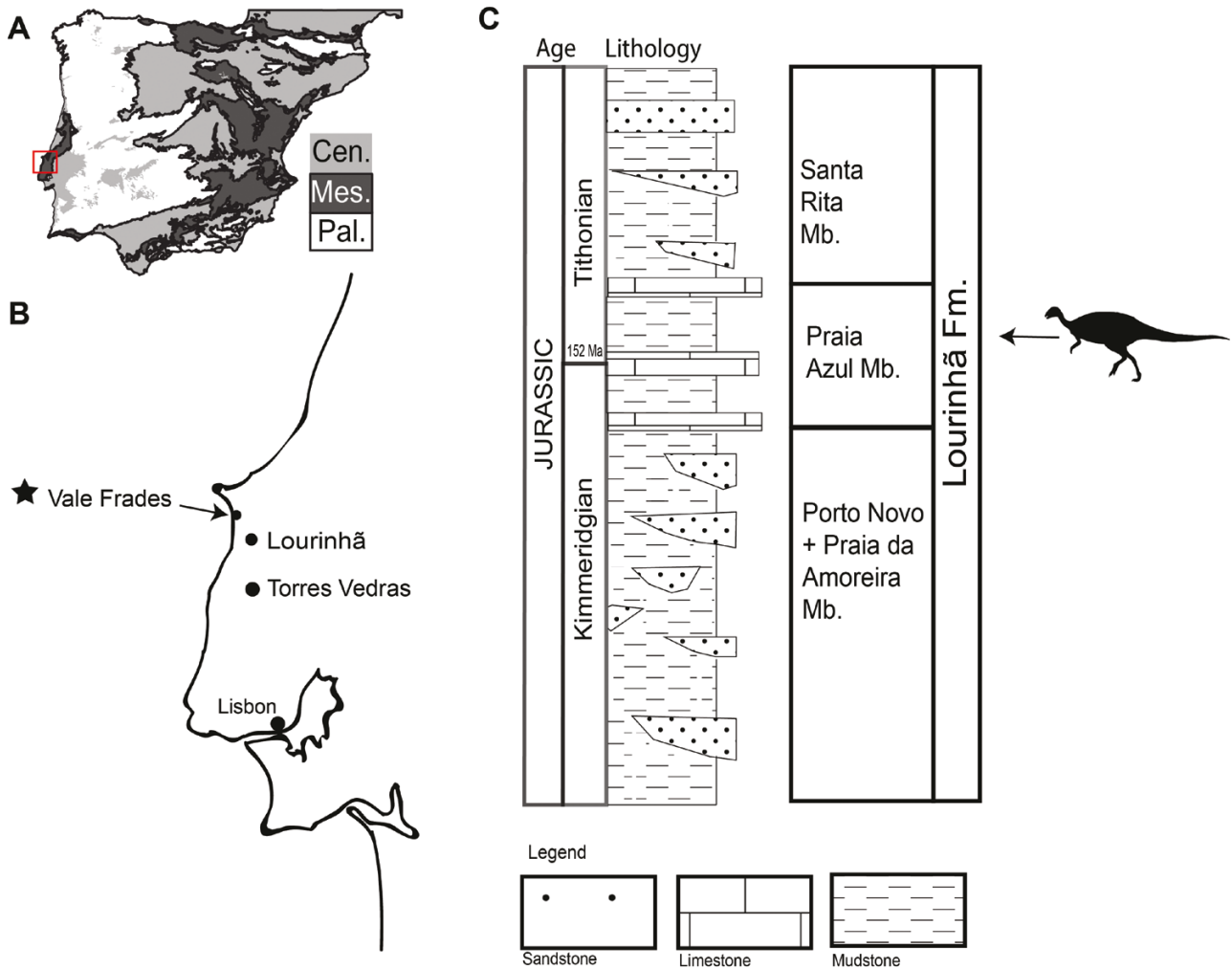


**Figure 1.** Geographical and geological settings of ML 357. A, B, Stratigraphic log of the Lourinhã Formation and position of the specimen. C, Re-adapted from Rotatori *et al.* (2020). Map of the Iberian Peninsula courtesy of Eduardo Puertolas-Pascual.

the fragments of rock attached to the bones of the new material, a dense grey muddy siltstone, are identical to that found encasing the old material, adding further support to the suggestion that it is part of the same individual. Both the old and new material of ML 357 have been prepared mechanically. Its post-cranium, except for the manual elements, has been subjected to CT-scanning in order to produce a three-dimensional model to illustrate its anatomy and better assess its phylogenetic characters. The specimen was first scanned at a veterinary facility, ‘Hospital veterinario do Oeste’, using a Siemens Somatom Emotion 6 with voltage set to 130 kV and a current of 200  $\mu$ A. To improve resolution of the first scan, the tarsus and pedal elements were re-scanned by the company ‘MiconSense’ using a GE VtomeX M 240, with voltage of 200 kV and a current of 500  $\mu$ A. It was not possible to segment the specimen, because of noise caused by permineralization due to diagenetic processes.

Therefore, the surface data were exported as 3D meshes by AVIZO v.9 in the free software BLENDER (Hess, 2010) and anatomical structures were isolated. As a third step, the specimen was articulated and rendered producing the images present herein.

To test its phylogenetic affinities, the old and newly reported material of ML 357, was first added to the dataset of Boyd (2015), followed by the modifications of Madzia *et al.* (2018) and Bell *et al.* (2018). We performed one global analysis, since the new material did not provide any new character scores. The analysis was carried out in TNT v.1.5 (Goloboff & Catalano, 2016), the tree search was performed in two steps, as described by Bell *et al.* (2018), and a ‘New Technology Search’ was conducted to find starting trees, setting 30 cycles of Drift and 50 cycles of Ratchet. Default options were used for the other parameters. The search was performed using 1000 random additional sequences. Subsequently, the most parsimonious trees (MPTs)

were subjected to an additional round of tree bisection reconnection (TBR) to further explore the tree-space.

After the first phylogenetic analysis confirmed the inclusion of ML 357 in Ankylopollexia, the specimen was added to the dataset of Xu *et al.* (2018) in order to explore its affinities within the clade. We corrected the scoring for character 121 of *Dryosaurus altus* Marsh, 1878, *Dysalotosaurus lettowvorbecki* Virchow, 1919 (scored as: 0), *Valdosaurus canaliculatus* Galton, 1975 and *Uteodon aphanocetes* (Carpenter & Wilson, 2008) (scored as '?') based on a literature review (Galton, 1981; Carpenter & Wilson, 2008; Barrett *et al.*, 2011; Barrett, 2016). As a tree-search strategy, we performed a heuristic search with 1000 replicates, keeping ten trees per replicate. The MPTs were then subjected to the TBR algorithm as in the previous search.

We investigated the variation of evolutionary rates across the topology obtained by the analysis of the dataset of Xu *et al.* (2018). We used the script for TNT developed by Rauhut & Pol (2019) to calculate the homoplasy concentration (HC) index, which is linearly related to an increase in evolutionary rates. The ages (FAD/LAD) of terminal taxa were downloaded from the Paleobiology Database on 19 January 2021, inserting the term Iguanodontia, and in case of multiple contradictory entries, we chose the age range with the greatest number of entries.

As an additional line of evidence, we performed a third set of analyses using Bayesian inference. We re-analysed the dataset of Xu *et al.* (2018) in the program MrBayes v.3.2.7 (Ronquist *et al.*, 2012) in two steps: first, we performed a non-clock analysis to calculate background evolutionary rate and then we proceeded to a clock analysis, time-calibrating the topology recovered from the non-clock analysis. The character evolution followed the Mk model (Lewis, 2001) and the values were sampled from a gamma distribution. The analysis sampled 10 000 000 generations per run, sampled with Markov chain Monte Carlo (MCMC) method for four runs of six chains per run. The initial 'burn-in' was set at 25%. Convergence of independent runs and stationarity were assessed through the program TRACER v.1.7.1 (Rambaut *et al.*, 2018) considering effective sample size (ESS) for each parameter informative with values equal or > 200. Then we proceeded to the clock-analysis according to the fossilized birth–death model (FBD; Heath *et al.*, 2014), under maximum diversity sampling tree methods corrected to exclude a sampled-ancestor model. The topology recovered from parsimony and non-clock analyses was implemented as strict prior. It employed the relaxed uncorrelated clock model independent gamma rate (IGR) and the background values for the clock-rates were sampled by a log-normal distribution. As in the previous analysis, character evolution followed the Mk model (Lewis, 2001) and the values were sampled from a gamma distribution.

The analysis sampled 10 000 000 generations per run, sampled with a MCMC method for four runs of six chains per run. The initial 'burn-in' was set at 25%. Convergence and stationarity were again assessed in TRACER v.1.7.1, adopting the same criteria described in the non-clock analysis. We provided a soft root upper prior (220, 205) for the tree, lower than the stratigraphic occurrence of the outgroup taxon (*Lesothosaurus diagnosticus* Galton, 1978) and being consistent with the ghost lineage of Ornithischia inferred by other works (Baron, 2019). Since MrBayes needs an extant taxon to perform the calculation of evolutionary rates, we set the occurrence interval for *Lesothosaurus diagnosticus* as (10, 0 Mya). We opted for this operation instead of creating a dummy taxon coded for just 0 because the matrix of Xu *et al.* (2018) is designed in a way that *L. diagnosticus* has this coding. The addition of a dummy taxon would create unnecessary noise within the topology and the rooting. Following Simões *et al.* (2020a, b), we implemented an informative prior for the base of the clock rate. This prior value is obtained by subdividing the median value for tree length in substitutions from posterior trees by the age of the tree, based on the median of the distribution for the root prior ( $4.0714/205.5 = 0.02$ ) (Simões *et al.*, 2020a, b).

We modelled rates based on a log-normal distribution, with the rates sampled from the log-normal distribution and the mean of the log-normal distribution given the value based on the non-clock tree estimate (0.02) in natural log scale =  $-3.9120$ . We chose to use the exponent of the mean to provide a broad standard deviation ( $e^{0.02} = 1.0202$ ). The terminal age uncertainty of the previously downloaded FAD/LAD was modelled according to a uniform prior.

In our attempt to reconstruct the body length of specimen ML 357, we used the linear equations introduced by Becerra & Ramirez (2018). We opted for the ones derived for metatarsal III, since it is the most complete and unaltered appendicular element in ML 357. In addition, Becerra & Ramirez (2018) categorized locomotory models of ornithischian dinosaurs as (1) cursorial, (2) subcursorial and (3) graviportal, based on the ratio of the femur and whole leg length. Ornithopods (including hadrosaurs) are considered to range from a cursorial to subcursorial locomotion stance. Since the hindlimb of ML 357 is not preserved in its integrity, we estimated the body length of ML 357 assuming a fully cursorial locomotory model according to the equation (1):

$$bl = -147.18 + 17.45 \times (m3)$$

Second, a subcursorial locomotory model according to the equation (2):

$$bl = -441.11 + 24.54 \times (m3)$$

Where *bl* is the estimated body length and *m3* is the linear measurement of the metatarsal III. The ecological implications of both models are discussed below in the Discussion. Selected measurements of ML 357 are provided in [Table 1. Supporting Information](#) including: TNT files of the parsimony analyses (Files S2, S3), the infiles of the non-clock (File S4) and clock-analysis (File S5) and a 3D model of the leg of ML 357 (File S6).

## RESULTS

### SYSTEMATIC PALAEOONTOLOGY

DINOSAURIA OWEN, 1842

ORNITHISCHIA SEELEY, 1887

ORNITHOPODA MARSH, 1881

IGUANODONTIA SERENO, 1986

DRYOMORPHA MILNER & NORMAN, 1984

ANKYLOPOLLEXIA SERENO, 1986

STYRACOSTERNA SERENO, 1986

*DRACONYX LOUREIROI* MATEUS & ANTUNES, 2001

(Figs 2–7)

*Type material:* The holotype specimen (newly reported material marked with \*), ML 357 (subnumbers from 1 to 31) includes two maxillary teeth, carpal bones, two metacarpal distal ends\*, three left carpal phalanges, one right carpal phalanx\*, two left unguals, three right unguals\* and one right leg including proximal femoral epiphysis, proximal and distal epiphysis of the tibia, astragalus, calcaneum, four metatarsals, five phalanges and two unguals.

*Referred specimen:* An isolated left femur, ML 434 from 1 km south of the type locality previously referred to *Draconyx loureiroi* by Mateus & Antunes (2001), now referred to *Ankylopollexia* indet.

*Type locality, horizon and age:* Vale de Frades, Lourinhã Municipality, Portugal. Praia Azul Member of Lourinhã Formation, lower Tithonian, 151–152 Mya.

*Emended diagnosis:* Styracosternan iguanodontian distinguished from other basal iguanodontians by the following combination of characters: unfused and non-interlocked carpus; absence of a sharp crest running from the medial condyle of the femur towards of the lesser trochanter, fully open U-shaped extensor groove on distal epiphysis of the femur; fully open V-shaped flexor groove without overhangs on distal epiphysis of the femur; concave medial margin of proximal epiphysis of the tibia; caudally pointing fibular condyle of the tibia; and a splint-like metatarsal I.

### Description and comparisons

*Cranial material: Maxillary teeth (ML 357–31) (Fig. 2A, B):* One of the maxillary teeth preserves part of the root and its crown is complete (Fig. 2A). The other tooth is just an isolated crown (Fig. 2B). The specimens appear to have suffered some erosion and post-mortem breakage. The root is slightly labiolingually curved and tapers smoothly into the crown (Fig. 2A). There is no cingulum at the junction between the root and the crown. Overall, the crown is leaf-shaped and the veneer of enamel is thicker on the labial side (Fig. 2A). Labially a thick primary ridge is distally offset and five accessory ridges are present on the mesial surface (Fig. 2A, B). Non-mammillated hook-like denticles are coarsely present on the mesial crown margin, while distally they appear to have been obliterated by either erosion or occlusal wear. An extensive occlusal surface develops on the apex of the crown and is inclined labiolingually approximately around 30° (Fig. 2A, B).

*Remarks:* The tapering root, slightly labiolingually recurved and the leaf-shaped crown are common characteristics of Dryomorpha (Galton, 1983, 2006; Norman, 1986, 2004). The maxillary crowns possess a distally offset primary ridge resembling the condition of ankylopollexians but differing from dryosaurids in which the primary ridge is located towards the centre of the crown (Galton, 2006). In the original description, Mateus & Antunes (2001) indicated the presence of five accessory ridges in the distal half of the crown as an autapomorphy of *Draconyx loureiroi*. However, the number of accessory ridges is variable throughout the dental series (Galton, 2006). Therefore, we regard it as a non-informative character if the tooth position is not articulated.

*Axial skeleton: Caudal vertebrae (ML 357–9–11) (Figs 3K–M, 4A–F):* Three proximal caudal vertebrae are preserved and, as for the rest of the skeleton, they have suffered breakage and erosion. The centra are stout and craniocaudally compressed. The largest centrum is ML 357–9, while ML 357–10 and ML 357–11 are slightly smaller. The cranial and caudal surfaces are slightly amphicoelous, having a subelliptical, rounded shape (Fig. 4 A, C, G, I, M, O). Dorsally, the neural arch preserves the ventralmost portion of the neural spine but the neural suture is not visible. Immediately caudal to the spine, in the most complete specimens ML 357–9 and ML 357–10, (Fig. 4C, O) two small, rounded and steeply inclined post-zygapophyses diverge laterally. On the lateral surface of the neural arch, the articulation for the transverse processes is overlain by a broken surface. The presence of this surface indicates that these vertebrae represent the cranialmost portion of the caudal series. In ventral





Table 1. Continued

Pedal Phalanx II-1 ML 357-17	50*	48	55
Pedal Phalanx II-2 ML 357-14	40	45	40
Pedal Phalanx III-1 ML 357-13	63	69	45
Pedal Phalanx III-3 ML 357-15	35	28	20
Pedal Ungual II ML 357-16	60	25	30
Pedal Ungual III ML 357-19	60	30	25

view, the centra have an hourglass-shaped outline (Fig. 4E, K, Q). The ventral surfaces of the centra possess a narrow keel and the margin is highly concave (Fig. 4B, P). Caudally, broad facets for chevrons are present.

*Remarks:* The three caudal vertebrae are stout and cylindrical, similar in overall shape and proportions to those of other basal iguanodontians, such as: *Camptosaurus dispar*, *Cumnoria prestwichii*, *Dryosaurus altus*, *Dysalotosaurus lettowvorbecki*, *Mantellisaurus atherfieldensis* Mantell, 1825 and *Uteodon aphanoecetes* (Galton & Powell, 1980; Galton, 1981; Norman, 1986; Carpenter & Wilson, 2008; Carpenter & Galton, 2018). They do differ remarkably from those of *Iguanodon bernissartensis* Van Beneden, 1881 and *Iguanacolossus fortis* McDonald et al., 2010b in being less discoidal in shape, and from *Barilium dawsoni* Lydekker, 1888a by being less compressed dorsoventrally (Norman, 1980, 2011; McDonald et al., 2010b).

*Manus (ML 357-1-5, 20-26) (Fig. 5):* The partial carpus (ML 357-5) is composed of the proximal part of a metacarpal, two distal carpals and a proximal carpal (Fig. 5A). Two isolated distal epiphyses of metacarpals (ML 357-25, 26) are associated with the semi-articulated carpus, being both consistent in size and their state of preservation (Fig. 5F, G). Four manual phalanges and five ungual phalanges are associated with the carpus (Fig. 5B-E). Three manual phalanges (phalanx n.2 ML 357-22, phalanx n.3 ML 357-21 and phalanx n.4 ML 357-24) and two unguals (ungual n.1 ML 357-1 and ungual n.4 ML 357-23) are likely to belong to the left manus (Fig. 4), while the remaining three unguals (ungual n.2 ML 357-2, ungual n.3 ML 357-3 and ungual n.5 ML 357-20) and manual phalanx n.1 ML 357-4 are attributed to the right manus. Given the fragmentary condition and the weathering of the specimen, it is not possible to identify the bones of each individual carpal. The two distal carpals are cuboid in shape and are stout elements, while the proximal carpal is more lightly built and slightly arched (Fig. 5A). The proximal end of the metacarpal preserves a concave proximal margin. Despite the poor preservation, it is possible to determine that the carpus does not include fused elements, as all of the contacts between all the identifiable carpals are clearly visible (Fig. 5A).

The two isolated distal metacarpals fragments are similar in shape: they are compressed along their extensor-palmar axis, broadening mediolaterally towards their distal ends. The medial and lateral ginglymi are subequal in size and preserved on their collateral ligament pits. The manual phalanges, ML 357-22 and ML 357-21, articulate with each other. Furthermore, phalanx ML 357-22 articulates with

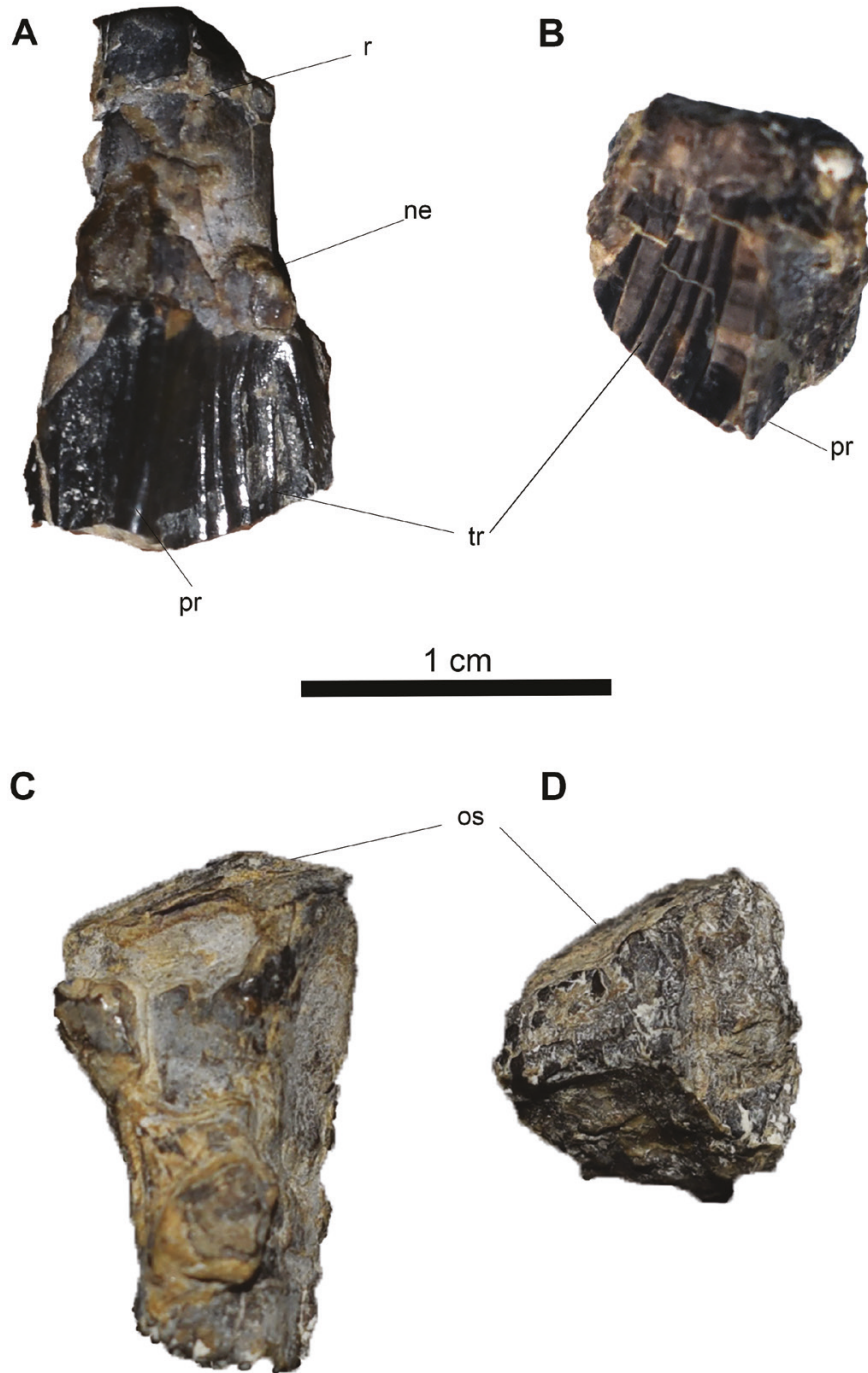


**Figure 2.** Two maxillary teeth of *Draconyx loureiroi* holotype ML 357 in labial and lingual views. Completely preserved maxillary in labial (A) and lingual (C) views; isolated maxillary crown in labial (B) and lingual (D) views. Abbreviations: ne: neck, os: occlusal surface, pr: primary ridge, tr: tertiary ridges.

the ungual ML 357–23. Therefore, these latter manual elements compose a complete finger (Fig. 5C, D, K). In general, all of the phalanges have a distal triangular section, moderately arched ventral surface and strongly inclined and robust ginglymi. The lateral ginglymus is smaller with respect to the medial one, with the

exception of phalanx n.2 where they are subequal (Fig. 5B–E). The unguals are generally elongated and claw-like, slightly arched along the extensor–palmar axis and have a subtriangular articular facet (Fig. 5H–L). The only exception, ungual n.5 (Fig. 5L), appears instead to be compressed along its extensor–palmar



**Figure 3.** General overview of *Draconyx loureiroi* holotype ML 357 post-cranial skeleton. Caudal vertebrae (K–M) in left lateral view. Right femur (A–E) in frontal (A), medial (B), caudal (C), lateral (D) and distal (E) views. Right tibia in medial (F) and lateral (G) views. Proximal end of the fibula in medial (I) and lateral (J) views. Right articulated pes in dorsal (N) and medial (Q) view. Pedal digit III (O) and pedal digit II (P) in dorsal view.

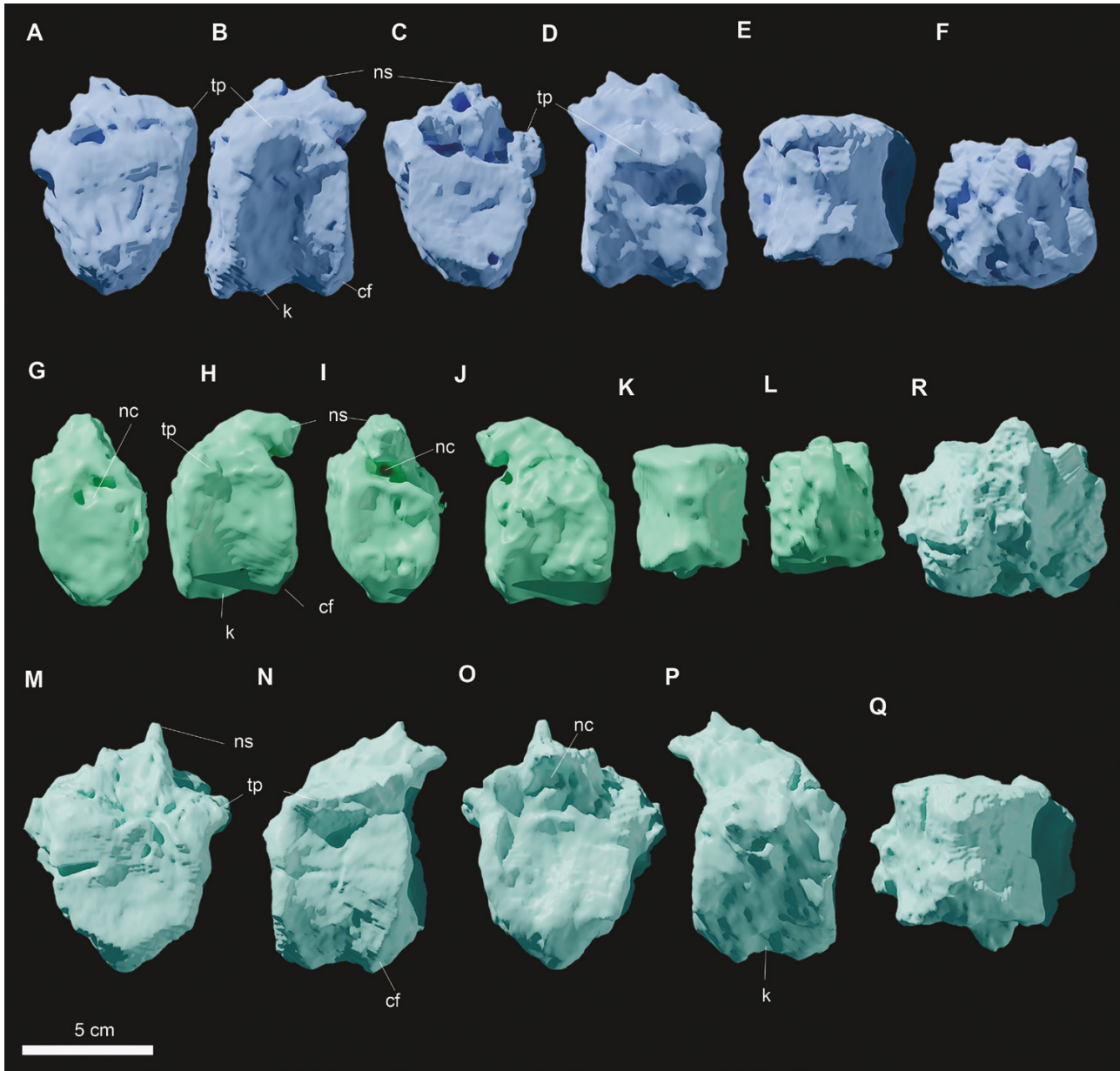


**Figure 4.** Three dimensional models of axial skeleton of *Draconyx loureiroi* holotype ML 357 (A–F): Caudal n.2 ML 357-10 in cranial view (A), left lateral view (B), caudal view (C), right lateral view (D), ventral view (E) and dorsal view (F). Caudal n.3 ML 357-11 (G–L) in cranial view (G), left lateral view (H), caudal view (I), right lateral view (J), ventral view (K) and dorsal view (L). Caudal n.1 ML 357-9 (M–R): cranial view (M), left lateral view (N), caudal view (O), right lateral view (P), ventral view (Q) and dorsal view (R). Abbreviations: cf: chevron facet, k: keel, nc: neural canal, ns: neural spine, tp: transverse process.

axis. A fracture develops mediolaterally and is slightly inclined craniocaudally. Both parts are separated by this fracture and have suffered mediolateral displacement.

**Remarks:** Despite the poor preservation of the carpus of ML 357, certain features allow comparisons with other taxa. The small metacarpals are not significantly different from those of other

iguanodontians (Norman, 2004). However, the carpus is constituted by isolated blocky elements, resembling the condition in dryosaurids and *Tenontosaurus* spp. (Dodson, 1980; Galton, 1981; Forster, 1990; Winkler *et al.*, 1997). The distal carpals of ML 357 differ from the ones of *Camptosaurus dispar*, which are arranged in two co-ossified and highly interlocked blocks. Furthermore, the carpus of ML 357 does not exhibit the total ossified condition present in *Iguanodon*

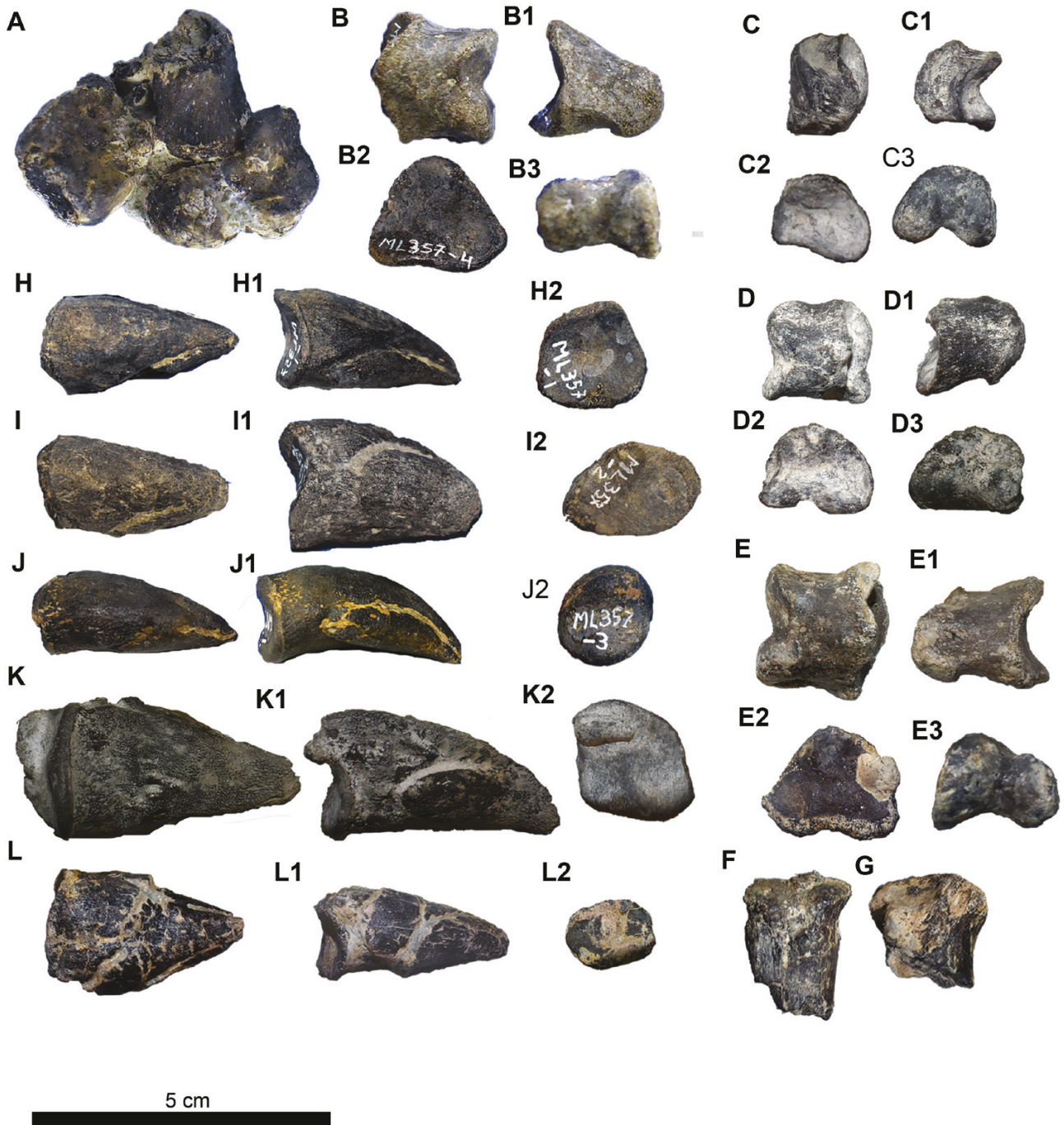


**Figure 5.** Manual elements of *Draconyx loureiroi* holotype ML 357 (ML 357 1-5, 20-26), including articulated partial carpus, manual phalanges and unguis (A–L). Articulated partial carpus (ML 357 – 5) in extensor view (A), right phalanx n.1 (ML 357 – 4) in dorsal view (B), lateral view (B1), proximal view (B2) and distal view (B3), left phalanx n.2 (ML 357 – 22) in dorsal view (C), lateral view (C1), proximal view (C2) and distal view (C3), left phalanx n.3 (ML 357 – 21) in dorsal view (D), lateral view (D1), proximal view (D2) and distal view (D3), left phalanx n.4 (ML 357 – 24) in dorsal view (E), lateral view (E1), proximal view (E2) and distal view (E3), isolated distal ends of tarsals (ML 357 – 25,26) in extensor view (F, G), left ungual phalanx n.1 in dorsal view (H), mediolateral view (H1) and proximal view (H2), right ungual phalanx n.2 (ML 357 – 2) in dorsal view (I), mediolateral view (I1) and proximal view (I2), right ungual phalanx n.3 (ML 357 – 3) in dorsal view (J), mediolateral view (J1) and proximal view (J2), left ungual phalanx n.4 in dorsal view (K), mediolateral view (K1) and proximal view (K2), ungual phalanx n.5 (ML 357 – 20) in dorsal view (L), mediolateral view (L1) and proximal view (L2).

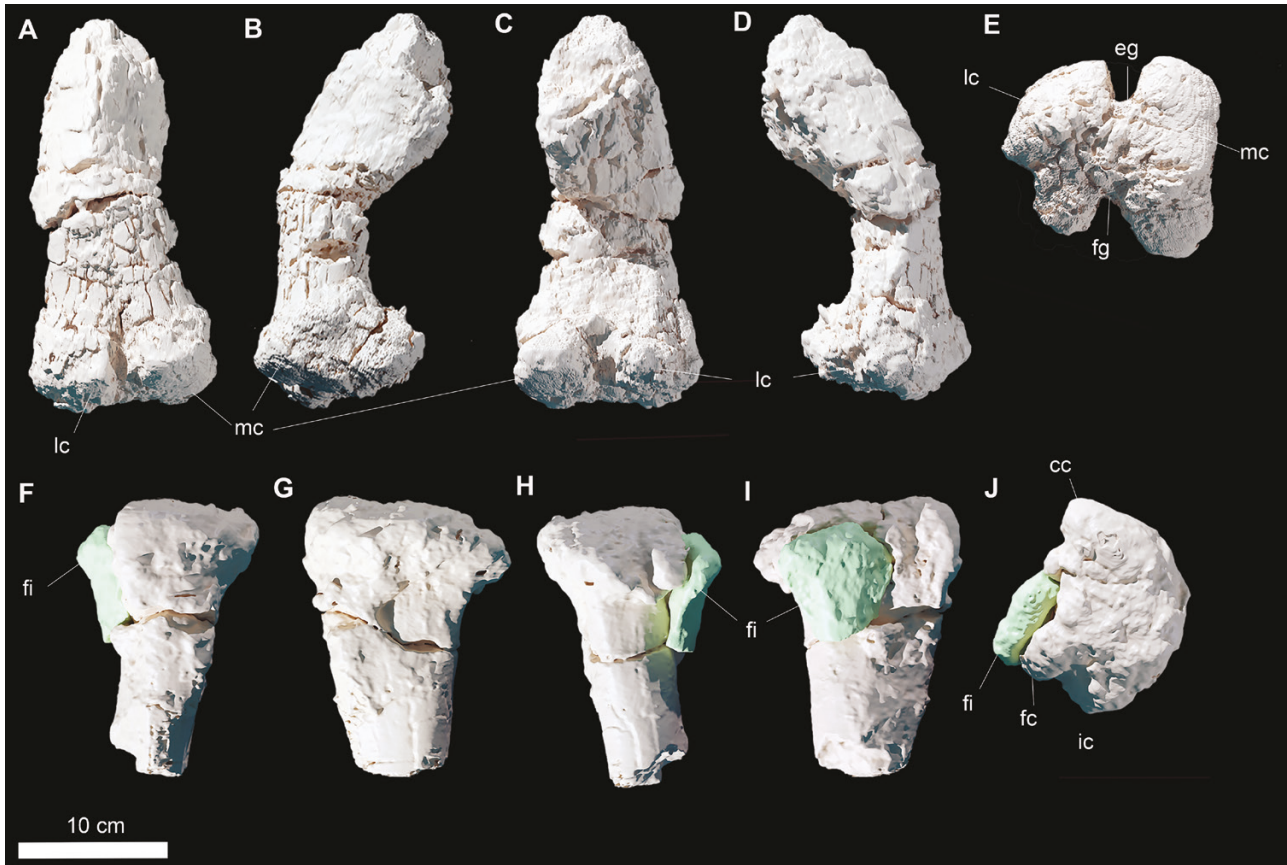


**Figure 6.** Three dimensional models of limb bones elements of *Draconyx loureiroi* holotype ML 357 (ML 357 6-8), femur (A–E) and tibia and proximal end of fibula (F–J). Femur (ML 357 – 6) in cranial view (A), medial view (B), caudal view (C), lateral view (D) and distal view (E). Tibia (ML 357 – 7) and proximal end of fibula (ML 357 – 8) in cranial view (F), medial view (G), caudal view (H), lateral (I) and proximal (J) views.

*bernissartensis*, *Magnamanus soriaensis* Vidarte *et al.*, 2016, *Mantellisaurus atherfieldensis* and other styracosternans (Fig. 12A–J) (Dodson, 1980; Norman, 1980, 1986, 2004, 2011, 2015, Vidarte *et al.*, 2016). The carpals and the manual unguals are similar to the ones present in *Camptosaurus dispar*, *Cumnoria prestwichii* and *Uteodon aphanoecetes*, differing from the ones of more derived styracosternans (i.e. *Iguanodon bernissartensis*, *Magnamanus soriaensis*, *Mantellisaurus atherfieldensis* and all other hadrosauriformes) in being, respectively, more arched and more claw-like instead of extremely compressed and hoof-like (Fig. 12A–J) (Galton & Powell, 1980; Norman, 1980, 1986, 2004; Carpenter & Wilson, 2008, Vidarte *et al.*, 2016).

**Femur ML 357–6 (Figs 3A–E, 6A–E):** The preserved right femur consists of the heavily eroded distalmost part of the shaft and the distal epiphysis. The

proximalmost part of the preserved shaft is mediolaterally crushed and compressed, due to taphonomic processes. The femur is strongly bowed craniocaudally; the section of the shaft was subcircular but is heavily distorted proximally by the compression and damaged distally (Fig. 6B, D). The distal epiphysis is subrectangular in shape in distal view, extending slightly more mediolaterally than craniocaudally. The two distal condyles are preserved, appearing subequal in size with the lateral condyle slightly larger than the medial one (Fig. 6E). A deep, extensive, fully open and U-shaped extensor groove separates the two condyles cranially (Fig. 6E). The cranial process of the lateral condyle is rounded and deflected caudally. The caudal finger-like process of the lateral condyle (condylid, according to Bertozzo *et al.*, 2017) is not preserved, being broken at its base, but the crest for the muscular insertion is distinguishable. The medial condyle appears stout

and rectangular, although its cranial and caudal process have been eroded. The flexor groove is fully open and its margin, consisting of the caudal process of the lateral condyle and the condylid of the medial condyle, are V-shaped in outline.

**Remarks:** The preserved femoral shaft is strongly bowed craniocaudally, as in dryosaurids, most elasmarians, *Camptosaurus dispar* and differently from *Tenontosaurus* sp. and other styracosternans (Norman, 1980, 1986, 2004; Carpenter & Wilson, 2008; Carpenter & Galton, 2018; Herne et al., 2019; Rozadilla et al., 2019, 2020). On the cranial surface there is no crest developing from the medial condyle, extending proximally towards the lesser trochanter, as seen in other ankylopollexians, such as *Camptosaurus dispar*, *Iguanodon* sp., *Mantellisaurus atherfieldensis* and *Uteodon aphanocetes* (Gilmore, 1909; Norman, 1980, 1986, 2004; Carpenter & Wilson, 2008; Carpenter & Galton, 2018). The lateral condyle of the distal epiphysis of the femur in *Draconyx loureiroi* is concave in outline and it extends more craniocaudally than the ones of *Camptosaurus dispar*, *Cumnoria prestwichii* and *Uteodon aphanocetes* (Fig. 7; Galton & Powell,

1980; Carpenter & Wilson, 2008). The inflection point of the curvature is located more cranially in *Draconyx loureiroi* than in *Camptosaurus dispar* and *Uteodon aphanocetes* (Carpenter & Wilson, 2008; Carpenter & Galton, 2018), while *Cumnoria prestwichii* exhibits a smoother outline without abrupt changes in curvature. The lateral condyle of Early Cretaceous species, such as *Barilium dawsoni* and *Mantellisaurus atherfieldensis*, are larger in proportions with respect to the total size of the epiphysis and extend more caudally than the ones of the above-mentioned taxa, including *D. loureiroi* (Norman, 1986; 2011). The medial condyle of *Draconyx loureiroi* is subrectangular and its medial margin is straight, as is the one of *Mantellisaurus atherfieldensis* and *Barilium dawsoni* (Norman, 1986; 2011). However, in Jurassic taxa such as *Uteodon aphanocetes* and *Camptosaurus dispar*, the medial margin of the medial condyle is rounded (Carpenter & Wilson, 2008; Carpenter & Galton, 2018). The flexor and extensor grooves are fully open as in many basal and cursorial iguanodontians, contrasting with more derived forms (Norman, 2004). Extensor grooves of the Jurassic taxa *Camptosaurus dispar* and *Uteodon aphanocetes* are fully open,

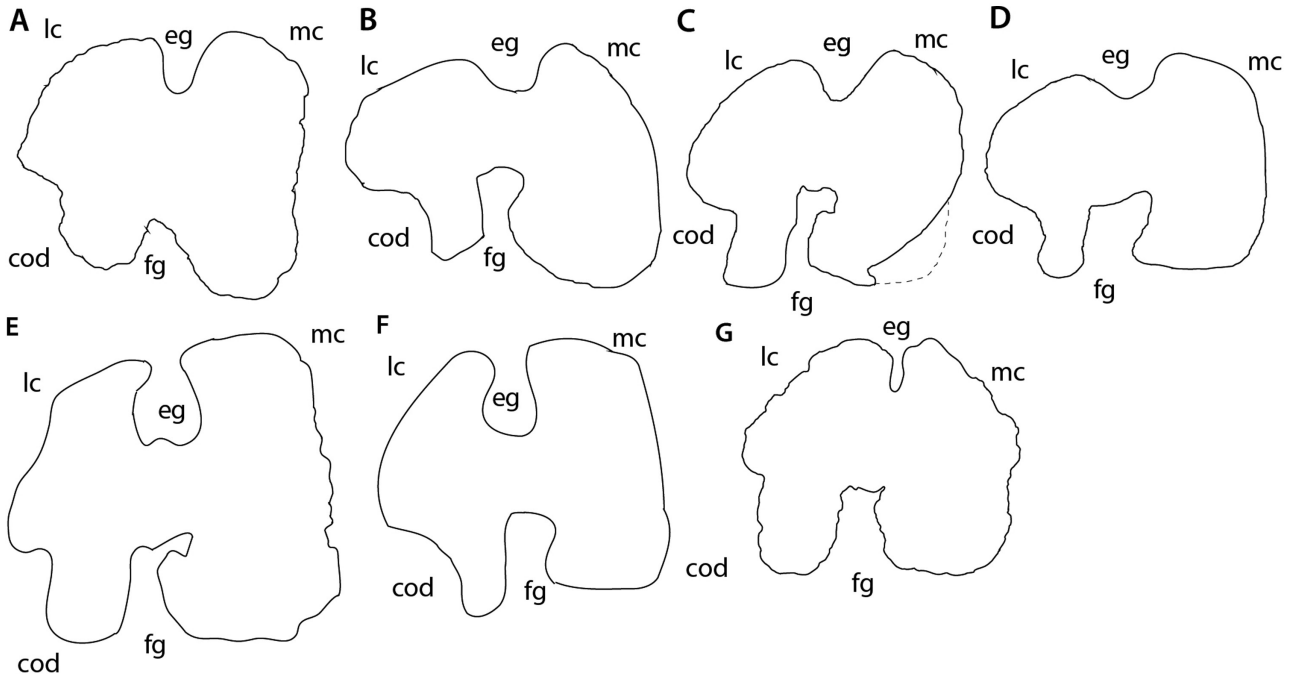


**Figure 7.** Comparison of distal sections of femoral shaft from selected iguanodontians. A, *Draconyx loureiroi*, B, *Uteodon aphanocetes*, C, *Cumnoria prestwichii*, D, *Camptosaurus dispar*, E, *Barilium dawsoni*, F, *Mantellisaurus atherfieldensis* and G, *Iguanodon galvensis*. Abbreviations: cod: condylid, eg: extensor groove, fg: flexor groove, lc: lateral condyle, mc: medial condyle. Distal sections drawn from: Carpenter & Wilson, 2008; Galton & Powell, 1980; Norman, 2011; Norman, 1986; Verdú et al., 2018.

but shallower compared to the ones of *Barilium dawsoni*, *Cumnoria prestwichii*, *Draconyx loureiroi*, *Iguanodon* sp. and *Mantellisaurus atherfieldensis* (Norman, 1980, 1986, 2004, 2011, Carpenter & Wilson, 2008; Carpenter & Galton, 2018; Verdú *et al.*, 2018). Moreover, the flexor groove walls of *Cumnoria prestwichii* and *Uteodon aphanocetes* are slightly divergent from one another (Fig. 7). The extensor groove of the Early Cretaceous iguanodontians *Barilium dawsoni*, *Mantellisaurus atherfieldensis* and other styracosternans are partially enclosed by overhangs of medial and lateral condyles. *Draconyx loureiroi* does not exhibit an overhang of the medial condyle on the flexor groove, unlike the condition present in *Camptosaurus dispar*, *Cumnoria prestwichii*, *Mantellisaurus atherfieldensis*, *Ouranosaurus nigeriensis* Taquet, 1976 and *Uteodon aphanocetes* (Norman, 1980, 1986, 2004, 2011; Carpenter & Wilson, 2008; Bertozzo *et al.*, 2017; Carpenter & Galton, 2018, Verdú *et al.*, 2018). This condition more closely resembles the plesiomorphic condition within Ornithopoda (Norman *et al.*, 2004).

**Tibia (ML 357–7, 12) (Figs 3F, G, 6F–J, 8A–D):** The proximal (Fig. 6F–J) and distal (Fig. 8A–E) epiphyses of the tibia are preserved, but the tibial shaft is missing. Both extremities are heavily eroded and covered by matrix and adhesives, but relevant characters are still distinguishable. The proximal epiphysis preserves a conspicuous cnemial crest, a robust fibular condyle and the internal condyle. The cnemial crest tapers dorsally forming a smooth edge; in dorsal view its margins are laterally concave and medially convex (Fig. 6G, I). Laterally, it is divided by the fibular condyle to form a deep and extensive scar (sulcus tibialis). The fibular condyle is a stout process that deflects strongly caudally, its articular facet is rounded and it blends smoothly with the anterior and posterior surfaces of the condyle. The internal condyle is a blunt eminence directed caudally and projecting gently laterally. Like the cnemial crest, its lateral margin is concave, while the medial margin is strongly convex (Fig. 6E). This convexity forms a deep sulcus that separates the internal condyle from the fibular condyle. Immediately ventral to the proximal epiphysis, the proximal part of the diaphyseal shaft is preserved and it is teardrop-shaped in cross-section. The distal part of the tibia is articulated with the astragalus, calcaneum and the metatarsals (Fig. 8A–E). The distal epiphysis flares mediolaterally, the medial malleolus is rounded and slightly more expanded mediolaterally than the lateral one, which is narrow and elongate, expanding proximodistally. They articulate between each other forming an angle of approximately 45°. The intermuscular line is located on the caudal surface of the distal epiphysis,

separating the surface of the two malleoli and reaching the astragalus, forming with its apex a continuous concave surface.

**Remarks:** The medial margin of the proximal epiphysis of the tibia is convex, as is typical of many iguanodontians (Norman, 2004), except for *Talenkauen santacrucensis* Novas *et al.*, 2004 and *Eousdryosaurus nanohallucis* Escaso *et al.*, 2014 (Escaso *et al.*, 2014; Rozadilla *et al.*, 2019; Dieudonné *et al.*, 2021). As noted by Dieudonné *et al.* (2021), the cnemial crest apex is directed strongly cranio-laterally, a characteristic common to Laurasian dryomorphans and *Dysalotosaurus* Pompeckj, 1920, differing from the condition exhibited by Elasmaria and the Portuguese ornithopod *Eousdryosaurus nanohallucis* (Escaso *et al.*, 2014). As in many styracosternans, the cnemial crest is well developed (Norman, 2004). The fibular condyle differs from dryosaurids (with the exception of *Valdosaurus canaliculatus*), *Camptosaurus dispar* and *Uteodon aphanocetes* in being partially posterolaterally deflected, similar to the condition seen in *Cumnoria prestwichii*, *Talenkauen santacrucensis* and more derived styracosternans (Galton & Powell, 1980; Norman, 1980, 1986, 2011; Norman *et al.*, 2004; Carpenter & Wilson, 2008; Barrett *et al.*, 2011; Rozadilla *et al.*, 2019). The distal epiphysis, found in articulation with the rest of the pes, does not differ significantly from that of other iguanodontians (Norman, 2004).

**Fibula (ML 357–8, 12) (Figs 3I, J, 6F–J, 8A–D):** The distal and proximal epiphyses of the fibula are preserved, whereas the diaphysis is completely absent. The proximal end is a flattened subtriangular element. Dorsally, it appears to be slightly medially convex. The cranial margin deflects abruptly dorsally into the cranial process, which is slightly eroded (Fig. 6I). In contrast, the caudal margin deflects less abruptly dorsally. A deep fossa is present close to the caudal margin on the lateral surface.

The distal epiphysis is in articulation with the rest of the pes, located on the lateral surface of the tibia and contacts the calcaneum (Fig. 7A–D).

**Remarks:** The proximal epiphysis has cranial and caudal margins that diverge smoothly, as in *Dryosaurus altus*, *Dysalotosaurus lettowvorbecki*, *Eousdryosaurus nanohallucis*, *Talenkauen santacrucensis* and *Valdosaurus canaliculatus*, but differs from *Iguanodon bernissartensis*, *Mantellisaurus atherfieldensis* and *Ouranosaurus nigeriensis* (Norman, 1980, 1986; Galton, 1981; Barrett *et al.*, 2011; Escaso *et al.*, 2014; Barrett, 2016; Bertozzo *et al.*, 2017; Rozadilla *et al.*, 2019). As in *Sektensaurus sanjuanboscoi* Ibiricu *et al.*, 2019 and *Talenkauen santacrucensis*, the caudal

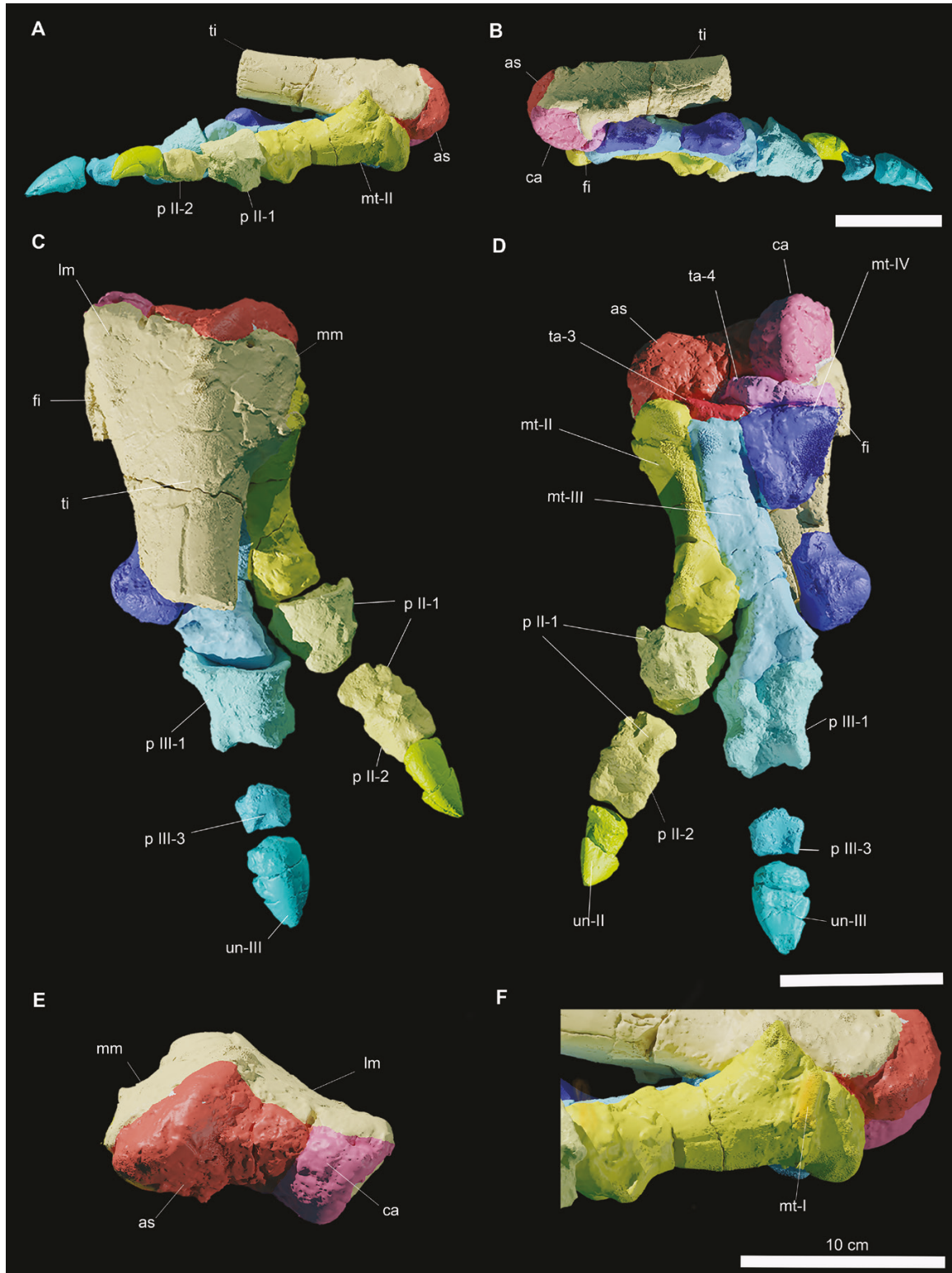


**Figure 8.** Three dimensional models of the pes of *Draconyx loureiroi* holotype ML 357. Articulated pes (ML 357-12) (A–F) in medial (A), lateral (B), dorsal (C), plantar (D) and caudal (E) views, F, detail of metatarsal I. Abbreviations: as: astragalus, ca, calcaneum, fi: fibula, lm: lateral malleolus, mm: medial malleolus, mt-I: metatarsal I, mt-II: metatarsal II, mt-III: metatarsal III, mt-IV: metatarsal IV, p II-1: pedal phalanx II-1, p II-2: pedal phalanx II-2, p III-1: pedal phalanx III-1, p III-2: pedal phalanx III-2, p III-3: pedal phalanx III-3, ta-3: tarsal 3, ta-4: tarsal 4, un-II: ungual II, un-III: ungual III.

margin of the proximal part of the fibula is almost vertical (Ibiricu *et al.*, 2019; Rozadilla *et al.*, 2019).

*Pes* (ML 357–12–19) (Figs 3N, Q, 8A–F, 9C, D): The pes is articulated with the distal tibia, distal fibula, astragalus and calcaneum and proximal metatarsals. The diagenetic permineralization between the tibia and the rest of the pes prevented a reliable segmentation by CT techniques. This also hampered views of the internal anatomy of the astragalus and calcaneum. The articulated elements share the same subnumber (ML 357–12), while the isolated elements have their own numbers. Therefore, the same element may have two subnumbers, depending on whether part of it belongs to the articulated block.

#### *Calcaneum*

The calcaneum is preserved in its entirety and does not show signs of significant breakage, erosion or distortion. In its general appearance, the calcaneum is a compact and narrow element, expanding

craniocaudally more than mediolaterally (Fig. 8B, E). Distally, its surface is subrectangular in outline and extends dorsally, appearing as a small rhomboidal element in caudal view (Fig. 8B, E). Caudally, the medial margin of the calcaneum forms a smooth concavity that accommodates the lateralmost margin of the astragalus. In lateral view, the calcaneum appears triangular with a caudal apex and is slightly deflected proximally. The proximal and distal margins progressively flare cranially, with the latter forming a scoop-like concavity.

#### *Astragalus*

Like the calcaneum, the astragalus is complete and not significantly distorted or eroded. In distal view, the bone has a subtrapezoidal shape (Fig. 8A, E). Laterally, it contacts the medial malleolus of the tibia via a deep concavity, while medially the astragalus/calcaneum contact is straight (Fig. 8A, E). In caudal view, the astragalus is triangular, with a high ascending process representing the apex, which protrudes extensively

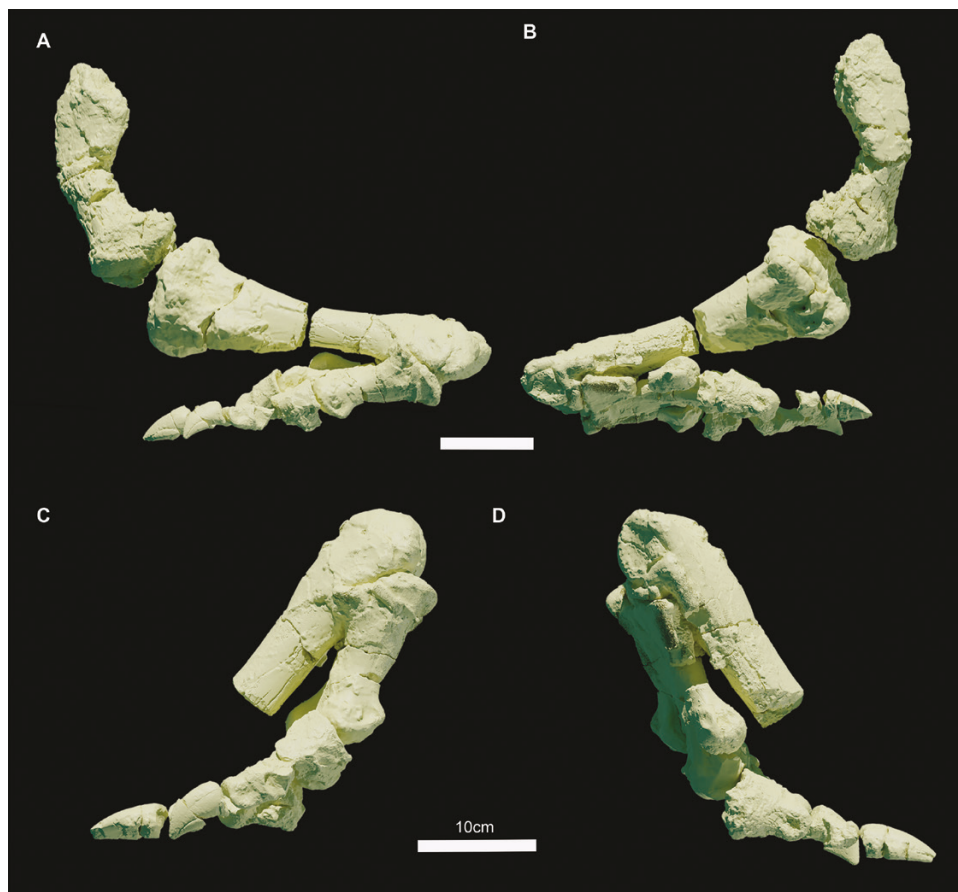


**Figure 9.** Three dimensional models of the articulated leg (A–B) and pes (C–D) of *Draconyx loureiroi* holotype ML 357. Leg in medial view (A) and lateral view (B). Pes in medial (C) and lateral (D) views.

dorsally. Immediately ventral to the ascending process, a stout steeply inclined caudomedial process forms a well-distinguishable relief.

*Remarks:* The astragalus of ML 357 is subtriangular and its caudal surface is moderately high, as in dryosaurids, *Camptosaurus dispar*, *Cumnoria prestwichii*, *Iguanodon bernissartensis* *Mantellisaurus atherfieldensis* and *Uteodon aphanacetes* (Galton & Powell, 1980; Norman, 1980, 1986; Galton, 1981; Carpenter & Wilson, 2008; Barrett *et al.*, 2011). The ascending process is not as developed as in *Barilium dawsoni*, *Iguanodon bernissartensis* or *Mantellisaurus atherfieldensis* (Norman, 1980, 1986, 2011), but more closely resembles the condition found in *Camptosaurus dispar* (NMNH 2210), *Cumnoria prestwichii*, *Ouranosaurus nigeriensis* and *Uteodon aphanacetes* (Galton & Powell, 1980; Carpenter & Wilson, 2008; Bertozzo *et al.*, 2017). As in the other known Portuguese ornithopod, *Eousdryosaurus nanohallucis*, it shows a caudomedial process, which casts doubt on the diagnostic status of this character for this latter taxon (Escaso *et al.*, 2014). The calcaneum does not possess any remarkable differences from other ankylopollexians (Norman, 2004).

#### Distal tarsals

Two distal tarsals are preserved, which are identified as tarsal 3 and tarsal 4 (Fig. 8D). Tarsal 3 is a large element that is mediolaterally elongated and contacts metatarsal III along a straight and linear surface (Fig. 8D). Tarsal 4 is a stout, elongated element and contacts the metatarsal IV along a concave surface, while its medialmost tip overlaps tarsal 3 proximally (Fig. 8D).

*Remarks:* Distal tarsals 3 and 4, found in articulation with metatarsals III and IV, resemble the ‘cushion-like’ condition described by Gilmore (1909) in *Camptosaurus dispar*, and differing from the thin-like and subrounded condition observed in *Iguanodon bernissartensis* and *Mantellisaurus atherfieldensis* (Norman, 1980, 1986) or the one present in basal ornithopods (Galton, 1974, 1981).

#### Metatarsus

Although they are fragmented, metatarsals II–IV are long and slender (Figs 8, 9C, D). A thick splinter of bone next to metatarsal II was interpreted as the proximalmost part of metatarsal I in the original description of Mateus & Antunes (2001) and a ‘vestigial digit I’ has been proposed as a possible autapomorphy for *Draconyx loureiroi*. Despite being heavily eroded, the bone is preserved in anatomical position and the rod-like structure supports the interpretation of this

bone as the first metatarsal (Fig. 8F). The status of this character as an ‘autapomorphy’ is discussed below. A deep groove in continuity with this fragment and impressed on metatarsal II probably represents the entire articulation surface with metatarsal I (Fig. 8F). Metatarsals II and III are complete and do not appear to have suffered extensive breakage or fracture (Fig. 8C, D). Metatarsal IV in contrast is broken at the midshaft with the distal epiphysis preserved as an isolated element.

#### Pedal digit I

The first pedal digit consists only of the splint-like metatarsal I (Fig. 8F).

#### Pedal digit II

Pedal digit II is represented by metatarsal II, the pedal phalanx II-1 (ML 357–17) and the ungual phalanx II-2 (357–16), which articulates with the phalanx II-2 (357–14). Pedal phalanx II-1 is broken at the midshaft, but the proximal and distalmost epiphyses are preserved (Fig. 8A, C, D).

Metatarsal II is positioned more proximally with respect to Mt III–IV. In mediolateral view, metatarsal II has a keyhole shape, as described by Herne *et al.* (2018) for the Australian ornithopod *Diluvicursor pickeringi* Herne *et al.*, 2018, with the proximalmost part dorsoplantarily higher than the distal epiphysis (Fig. 8A, F). The distal epiphysis develops more dorsoplantarily than mediolaterally, and the articular surface is convex. The shaft of Mt II is piriform (teardrop) in cross-section, with the plantar surface bearing a keel. The distalmost part of the epiphysis expands dorsoplantarily, giving the condyle a subtrapezoidal outline (Fig. 8A, D). The condyle of the metatarsal articulates perfectly with pedal phalanx II-1, which accommodates the condyle in a gently convex triangular facet. The distal epiphysis of the phalanx is in articulation with pedal phalanx II-2, which is a thick, subrectangular element in dorsal view (Fig. 8C, D). Proximally, the articular facet is not visible, but distally the two condyles are well distinguishable, the lateral slightly inclined with respect to the medial one. On both lateral surfaces, deep extensor grooves are present for tendon insertion. The ungual (phalanx II-2) of the pedal digit II is preserved, being a pointed claw-like element, which is dorsoplantarly arched and proximodistally elongated (Fig. 8A, C, D).

#### Pedal digit III

Pedal digit III is composed of metatarsal III, the largest pedal phalanx preserved III-1 (ML 357–13), the smallest pedal phalanx is interpreted to be III-3

(ML 357–15) and the largest ungual, pedal phalanx III-4 (ML 357–19). The pedal phalanx III-2 is missing. Metatarsal III is the longest element of the metatarsus, being a slender, yet compact element. Proximally, the Mt III articulates with the tarsal 3 and intervenes between Mt II and Mt IV (Fig. 8B–D). The subrectangular shaft ends distally in a mediolaterally expanded condyle, the only metatarsal exhibiting this condition. Pedal phalanx III-1 is a stout, robust element, which is moderately dorsoplantarly arched. The proximal articular facet is concave and subellipsoidal in outline, being the long axis oriented mediolaterally (Fig. 8B–D). Distally, the two ginglymi are subequal in size, being marked by deep collateral ligament pits. Pedal phalanx III-3 is a small proximodistally compressed element, which possesses a dorsoplantarly deep articular facet (Fig. 8B–D). The ventral margin of pedal phalanx III-3 is not as arched as the other phalanges and the collateral ligament pits occupy almost the entire lateral and medial surfaces. The ungual of the digit III (pedal phalanx III-3) is a stout, pointed element, which is more robust than the ungual preserved on pedal digit II. The ungual of digit III differs also from the other preserved ungual in having a less arched and more dorsoplantarly flattened outline (Fig. 8B–D).

#### *Pedal digit IV*

Metatarsal IV (ML 357–12, 18) is the only element of pedal digit IV available. Proximally it is the most mediolaterally expanded and dorsoplantarly compressed of the metatarsals and the proximal epiphysis is fan-shaped in dorsal and plantar view (Fig. 8B–D). Distally, the section of the shaft becomes progressively subrectangular, culminating in a moderately dorsoplantarly deep distal condyle (Fig. 8B–D).

*Remarks:* The metatarsus of ML 357 differs strongly from those of *Camptosaurus dispar*, *Iguanodon bernissartensis*, *Ouranosaurus nigeriensis*, *Uteodon aphanocetes* and other large-sized hadrosauriforms in general proportions, while exhibiting the slender and gracile proportions seen in *Cumnoria prestwichii* and *Mantellisaurus atherfieldensis* instead (Gilmore, 1909; Galton & Powell, 1980; Norman, 1980, 1986, 2004; Bertozzo *et al.*, 2017). Furthermore, as in the latter taxa, ML 357 possesses a metatarsal III that is sensibly more elongated with respect to metatarsals II and IV (Galton & Powell, 1980; Norman, 1986). This is in stark contrast to elasmarians *Camptosaurus dispar*, *Cumnoria prestwichii*, *Dryosaurus altus* and *Dysalotosaurus lettowvorbecki*, whose metatarsal I is extremely reduced, losing any functional capability (Gilmore, 1909; Galton & Powell, 1980; Galton, 1981;

Carpenter & Galton, 2018). However, this condition is preserved in some specimens of *Iguanodon bernissartensis* and *Mantellisaurus atherfieldensis* (Norman 1980, 1986). Assessing the presence of this character in other taxa is problematic, because of the extreme fragility of the reduced metatarsal I, whose absence/presence is highly subject to preservation bias. The alleged dryosaurid, *Eousdryosaurus nanohallucis*, from the same formation as ML 357, has been shown to possess a reduced metatarsal I in articulation with a pedal phalanx (Escaso *et al.*, 2014).

#### PREVIOUSLY REFERRED SPECIMENS

##### *Ankylopollexia indet.*

*Femur ML 434 (Fig. 10):* Mateus & Antunes (2001) referred an isolated femur (ML 434) to *Draconyx loureiroi*, based on geographical proximity. ML 434 is an almost complete and undistorted left femur, but lacks part of its proximal epiphysis and its entire distal one. The femoral shaft is stout and robust in general proportions and appears strongly bowed craniocaudally in lateral view, but is straight in cranial view. The cross-section of the shaft is subovoidal, with a sharp edge that corresponds with a ridge that extends dorsoventrally from the medial condyle. Proximally, only a part of the femoral head is preserved, which is gently deflected medially. At approximately the midshaft on the medial surface of the femur, a pendant fourth trochanter is present, its broad base forming an elongated crest-like surface. The scar for the insertion of the musculus caudifemoralis longus is located immediately cranial to the trochanter, being separated from the eminence of the trochanter. Distally, the eroded epiphysis preserves the general appearance of the two condyles, although the proportions with respect to one another are unclear. Parts of the flexor and extensor grooves are preserved caudally and cranially. A well-defined, sharp crest runs proximodistally from the medial condyle towards the location of the lesser trochanter.

*Remarks:* ML 434 possesses a strongly craniocaudally bowed femur and a pendant-like fourth trochanter as in the dryosaurids *Camptosaurus dispar* and *Uteodon aphanocetes* (Galton, 1981; Carpenter & Galton 2018). The base of the fourth trochanter is located at the midshaft of the femur, as is commonly found in *Ankylopollexia*, but different from *Dryosauridae*, in which this structure is confined to the proximal part of the shaft (Norman, 2004). Similar to *Camptosaurus dispar*, *Cumnoria prestwichii*, *Uteodon aphanocetes* and *Valdosaurus canaliculatus*, the scar of the m. caudifemoralis longus reaches the base of the fourth trochanter. Moreover, the morphology of the ridge

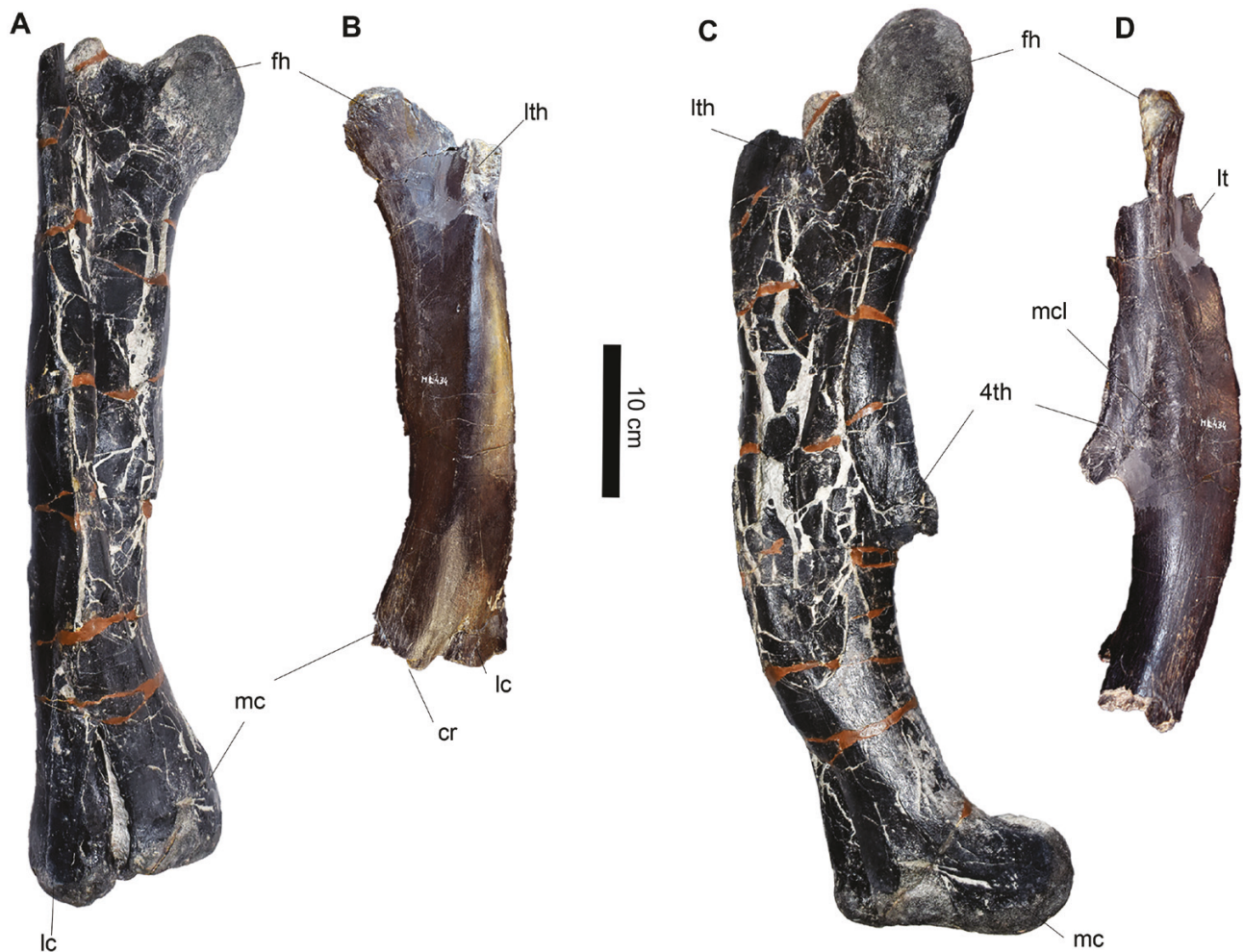


**Figure 10.** Comparison between the left femur ML 434 and the right femur SHN.(JJS).15. Femur SHN.015 and ML 434 in cranial (A, C) and medial (B, D) view. Abbreviations: 4th: fourth trochanter, cr, crest, fh, femoral head, lc, lateral condyle, lt, lesser trochanter, mc, medial condyle, mcl, scar of the *Musculus caudifemoralis longus*.

formed by the base of the fourth trochanter is similar to the one of the specimen SHN.(JJS).15 (Fig. 10A, D), which is not referable to *D. loureiroi* (Escaso, 2014) based on its partially enclosed flexor and extensor groove. The crest running from the medial condyle proximally towards the lesser trochanter is a character shared with a plethora of other iguanodontians (Gilmore, 1909; Carpenter & Wilson, 2008), including with SHN.(JJS).15, but not with the holotype of *Draconyx loureiroi*. Thus, ML 434 should be regarded as *Ankylopollexia indet.* based on the pendant fourth trochanter, the base of the fourth trochanter located at the midshaft and the scar of *m. caudifemoralis longus* reaching the base of the fourth trochanter.

#### PHYLOGENETIC ANALYSIS

Analysis of the Bell *et al.* (2018) dataset returned 99.999 MPTs (consistency index = 0.340; retention

index = 0.638) with length of 920 steps (Fig. 11). The strict consensus tree lacks sufficient resolution for any meaningful discussion, so we identified wildcard taxa using the iterpcr algorithm (Pol & Escapa, 2009) implemented in TNT v.1.5. This led us to pruning a posteriori the following taxa: *Atlascopcosaurus* Rich & Vickers-Rich 1989, *Burianosaurus* Madzia *et al.*, 2017, *Changchunsaurus* Zan *et al.*, 2005, *Gideonmantellia* Ruiz-Omeñaca *et al.*, 2012, *Haya* Makovicky *et al.*, 2011, *Leaellynasaura* Rich & Rich, 1989, LRF 50, *Lycorhinus* Hughton, 1924, *Macrogyposaurus* Calvo *et al.*, 2007, *Micropachycephalosaurus* Dong, 1978, *Mochlodon vorosi* Ósi *et al.*, 2012, *Notohypsilophodon* Martínez, 1998, *Qantassaurus* Rich & Vickers-Rich, 1999, *Stenopelix* Meyer, 1857, *Thescelosaurus garbanii* Morris, 1976 and *Weewarrasaurus* Bell *et al.*, 2018. The general topology does not differ from the one recovered by the original analysis of Bell *et al.* (2018).

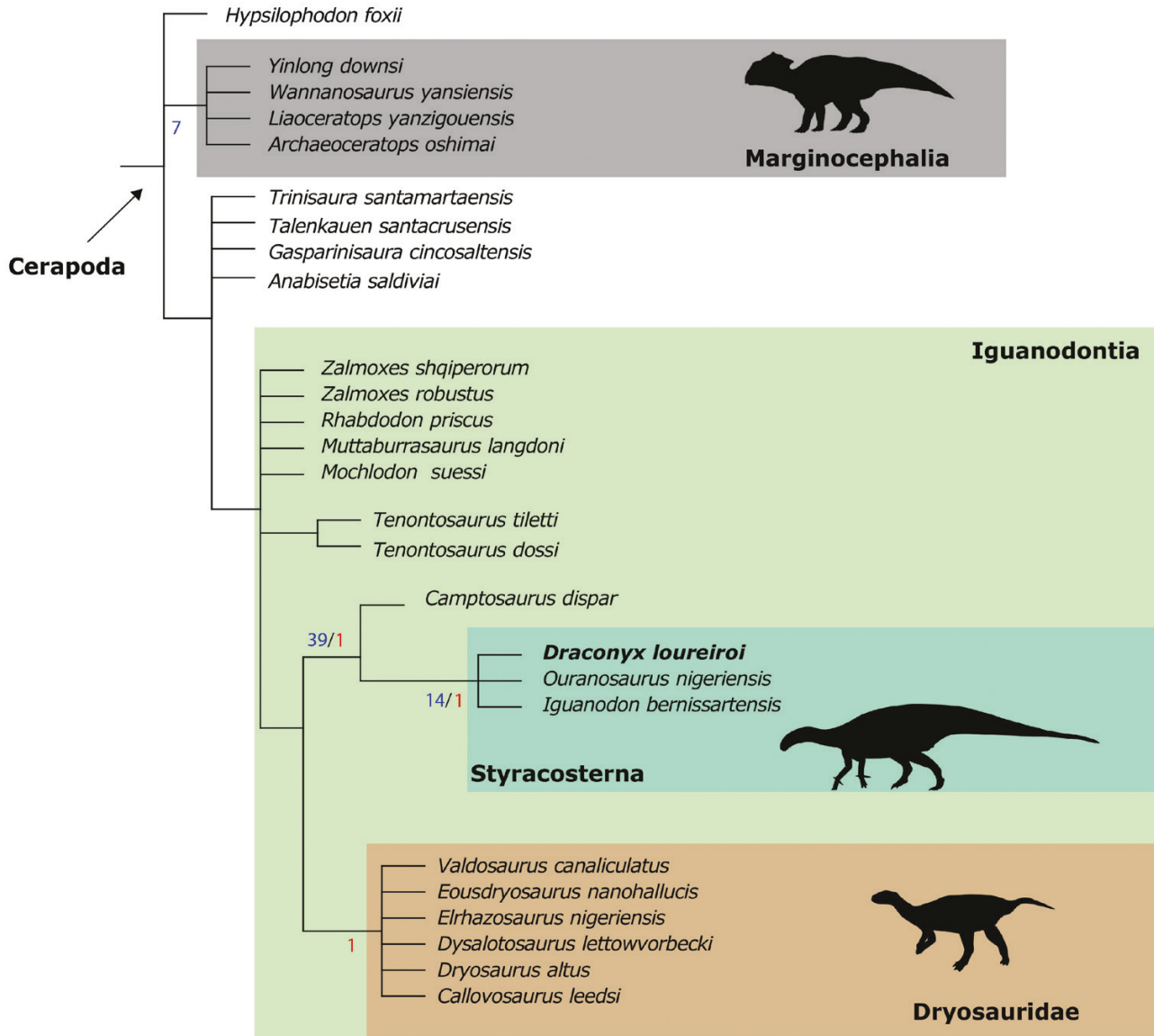


**Figure 11.** Pruned strict consensus tree of the parsimony analysis of the dataset of Bell *et al.* (2018). Bootstrap value in blue, Bremer support in red. Silhouettes from phylopic.org. Credit: Nobu Tamyra, Matthew Dempsey and Gareth Monger.

ML 357 is recovered within Styracosterna, more deeply nested than *Camptosaurus dispar* in a polytomy with *Iguanodon bernissartensis* and *Ouranosaurus nigeriensis*. The inclusion of ML 357 into Styracosterna is based on the presence of a sharply defined cnemial crest (Char. 231:1).

The inclusion of ML 357 into the dataset of Xu *et al.* (2018) gave consistent results with the previous analysis (Fig. 11A), recovering the specimen in Styracosterna as sister to *Dakotadon lakotaensis* (Weishampel & Bjork, 1989), returning a single tree of 311 steps (CI = 0.627; RI = 0.893). The general tree topology and the supporting synapomorphies for the nodes of Ankylopollexia and Styracosterna do not differ

from the original study of Xu *et al.* (2018). Styracosterna is supported by the following synapomorphies: a conical mediolaterally enlarged ungual on manual digit I (Char. 92:1) and a subtriangular section of the femoral shaft (Char. 116:1). The inclusion of ML 357 in Styracosterna is due to the presence of a splint-like metatarsal I (Char. 121:1). In the present analysis, the genus *Camptosaurus* as defined by Carpenter & Galton (2018) was not recovered, therefore, it follows the taxonomic revision of McDonald (2011) and considers *Cumnoria prestwichii* and *Uteodon aphanoecetes* as distinct genera.

The Bayesian non-clock analysis, including ML 357 in Xu *et al.* (2018), found the same tree topology as

the maximum parsimony analysis [see the output maximum compatibility tree (MCT) in Fig. 13]. The effective sample size (ESS) value for all parameters is  $> 200$ , indicating the good quality and the stationarity phase reached by the analysis. Furthermore, the potential scale reduction factor (PRSF) is equal to 1 for all parameters and the average standard deviation of split frequencies (ASDSF) value is  $\sim 0.004$ , supporting the interpretation indicated by the ESS values. The marginal likelihood obtained in the non-clock analysis is  $-1381.99$  (harmonic mean).

The clock analysis, including the topology of the non-clock analysis implemented as strict prior, obtained parameters ESS values generally  $> 200$ . In addition, PRSF values for the parameters range from 1.000 to 1.001 and an ASDSF value of 0.0000, confirming that convergence and stationarity in our analysis have been achieved. The marginal likelihood obtained in the clock analysis is  $-1390.60$  (harmonic mean).

#### EVOLUTIONARY RATES

The analysis (Fig. 12A–C) of the HC within the topology obtained by the parsimony analysis of the dataset of Xu *et al.* (2018), located high rates of homoplasy in various parts of the tree. As is evident in this analysis, and already pointed out by Rauhut & Pol (2019), HC peaks and evolutionary rates' acceleration are directly correlated (Fig. 12C, D). The highest peak, as indicated by the XY graphs, is at the base of the tree and further back in time. This is because the outgroup, *Lesothosaurus diagnosticus*, is selected as extant by the script in order to calculate evolutionary rates through time. Therefore, this is an artefact produced by the analysis. However, the analysis located two peaks of HC in this topology: the first is at the base of Dryomorpha (Ankylopollexia + Dryosauridae) and the other is deeply nested in Hadrosauroidea.

The first peak is located approximately between 145 and 135 Mya, comprising the appearance of several basal styracosternan lineages. This shift encompasses the Jurassic–Cretaceous transition, which is generally characterized by peculiar patterns of faunal turnovers and radiations among different groups (Tennant *et al.*, 2017). The small inflection at 140 Mya may be due to sampling biases in the fossil record occurring during the earliest stages of the Cretaceous (Tennant *et al.*, 2017). The second peak, located at approximately around 80 Mya, is related to the appearance of Rhabdodontidae and derived hadrosauroids. High HC rates in the clade Rhabdodontidae are most probably due to their long ghost lineage and early divergence time from the rest of Iguanodontia. The appearance of the high HC rates within Hadrosauroidea is linked to the appearance of more derived Late Cretaceous

forms, as noticed by Stubbs *et al.* (2019), and related increases of morphospace occupation.

The Bayesian inference results do not contradict the ones obtained from parsimony analysis (Fig. 13). The clock analysis revealed acceleration in the evolutionary rates across a wider time range between 170–140 Mya and around 80 Mya, recovering essentially the same signal described above. However, there are slight differences between the results of the two methodologies. First, the time range linked to the radiation of basal styracosternans is essentially longer and 5 Myr offset with respect to the previous analysis. This is due to the different ways of MrBayes and TNT script to model age uncertainties: the first models this parameter according to a uniform distribution, while the second creates a discrete time-bin (Ronquist *et al.*, 2012; Rauhut & Pol, 2019). Second, it does not recover the increase of evolutionary rates within Rhabdodontidae. However, it does support the previous analysis in suggesting that the main radiation of basal styracosternans occurred across the Jurassic–Cretaceous transition and the relative acceleration of evolutionary rates, coinciding with the appearance of derived hadrosauroids.

#### LENGTH ESTIMATION

The application of the fully cursorial model, given the scalar value of 175 mm for metatarsal III, produces a length estimate of 2906 mm, while the subcursorial model produces an estimate of 3853 mm. Therefore, the length ranges between 3 and 4 m. Waskow & Mateus (2017) showed that ML 357 was a senile specimen, approximately 30 years old. Therefore, our estimation represents the maximum length that the species *Draconyx loureiroi* reached at the end of its ontogenetic development. This length estimation contrasts with individuals of *Camptosaurus dispar*, *Iguanodon bernissartensis* and *Mantellisaurus atherfieldensis* that reached end of life-history lengths of up to 7–9 m (Norman, 1980, 1986; Erickson, 1988). The estimated length for *Draconyx loureiroi* is similar to that of *Cumnoria prestwichii*, reported by Galton & Powell (1980) to be around 4–5 m, even though there is no evidence that the holotype of *C. prestwichii* pertains to a fully mature individual. Therefore, we can consider *Draconyx loureiroi* as a relatively small styracosternan species, compared to its closest relatives.

#### DISCUSSION

##### SYSTEMATIC POSITION OF *DRACONYX LOUREIROI* (ML 357)

ML 357 has been recovered nested in Styracosterna using the Bell *et al.* (2018) and Xu *et al.* (2018) datasets. Both analyses, as in many cases for the

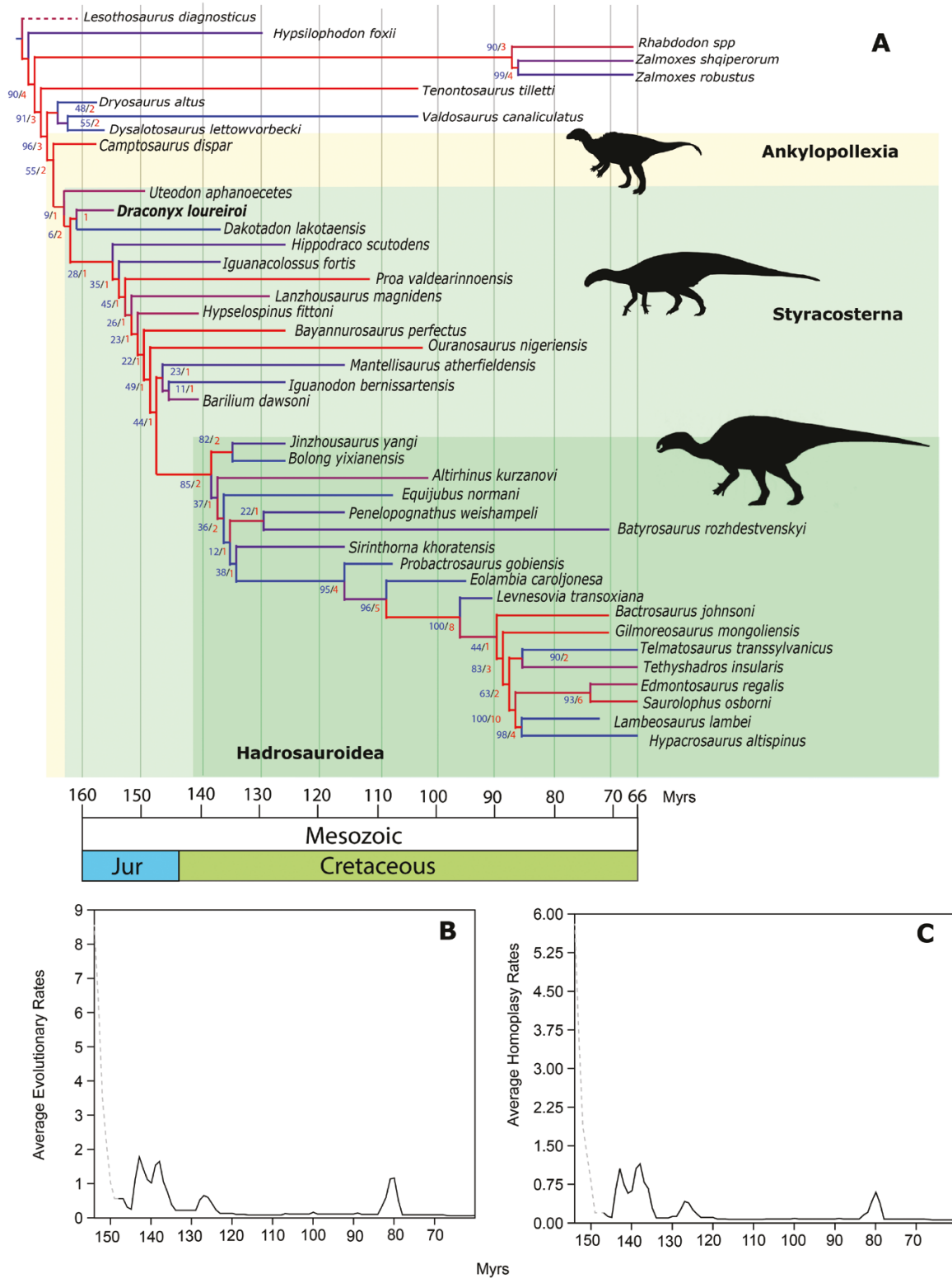


**Figure 12.** Time calibrated strict consensus tree of the analysis including *Draconyx loureiroi* in the dataset of Xu et al. (2018) (A). Bootstrap value in blue, Bremer support in red. Red colour is associated with an increasing Homoplasy Concentration index. XY graphs of Average Evolutionary Rates (B) and Average Homoplasy Rates (C) through time. Note the coinciding peaks of both AER and AHR. Silhouettes from phylopic.org. Credit: Michael Keesey, Matthew Dempsey and Pete Buchholz.

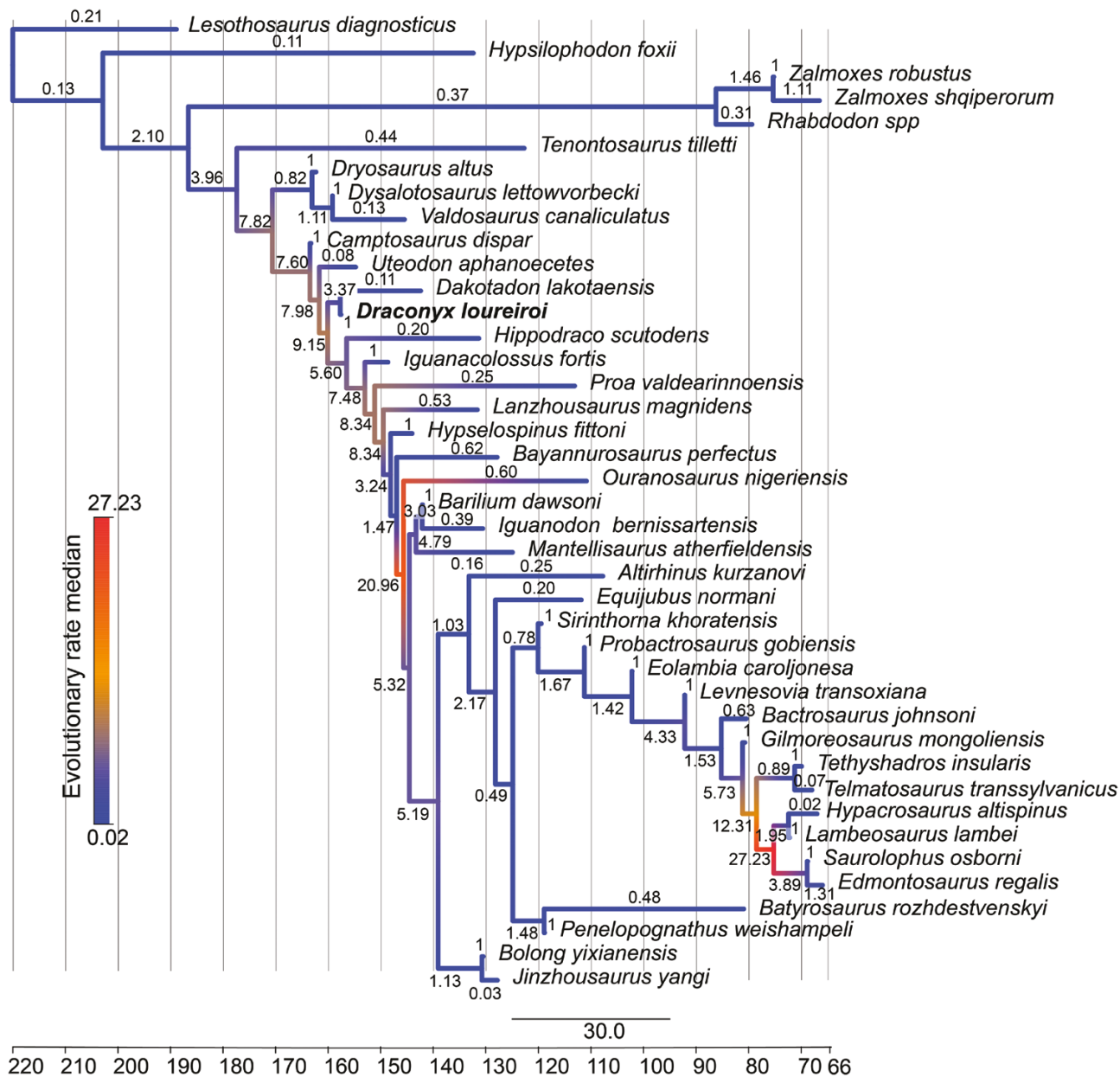


**Figure 13.** Time calibrated Maximum Compatibility Tree (MCT) of the Bayesian clock analysis of the dataset of Xu *et al.* (2018). Colours of the branches reflect median evolutionary rates and number represents absolute values along branches themselves.

base of Iguanodontia, are not strongly supported. The inclusion of ML 357 in Styracosterna is due to the development of the cnemial crest or the presence of a splint-like metatarsal I, depending on the dataset used. In the original description of Mateus & Antunes (2001), a ‘vestigial metatarsal I’ was proposed as a possible autapomorphy for this species. However, as pointed out in the comparisons, a reduced metatarsal I is common to many styracosternans, although these analyses did not recover it as a common synapomorphy for the

clade. The development of the cnemial crest in ML 357 is regarded as a synapomorphy for Styracosterna. However, this character state does not appear to support the inclusion of ML 357 in other nodes in the matrix. The data matrix of Bell *et al.* (2018) broadly samples Ornithischia, so we consistently consider it diagnostic.

Other characters that support the styracosternan affinities of ML 357 are the fibular condyle of the tibia, which is caudally deflected, as observed in *Iguanodon*

*bernissartensis*, *Mantellisaurus atherfieldensis* and *Ouranosaurus nigeriensis* (Norman, 1980, 1986; Bertozzo *et al.*, 2017). Verdú *et al.* (2018), in their phylogenetic analysis of *Iguanodon galvensis* Verdú *et al.*, 2015, recovered *Draconyx loureiroi* in an unresolved polytomy in Styracosterna, supporting the present interpretation of ML 357 as a styracosternan iguanodontian.

Beside the characters supporting its affinities with Styracosterna, *D. loureiroi* ML 357 possesses a combination of characters that indicate a complex evolutionary history for iguanodontians. The carpus is not closely packed, as it occurs in dryosaurids and the styracosternan *Uteodon aphanocetes*, contrasting with the closely packed and interlocked condition of carpal elements in *Camptosaurus dispar* (Fig. 14A, B, D, E, G, H). Also, the carpal bones are not fused as in derived styracosternans, such as *Iguanodon bernissartensis*, *Mantellisaurus atherfieldensis* or *Magnamanus soriaensis* (Fig. 14C, F, I) (Norman, 2004). Generally, the fused condition of the carpus is associated with the presence of the hypertrophied conical thumb (spike), which is typical for many Early Cretaceous styracosternans (Norman, 2004). Ankylopollexians present unguals just in the first three manual digits (Norman, 1980, 1986; Carpenter & Wilson, 2008), ML 357 presents five out of six unguals for both hands,

none of them resembling the morphology of the conical thumb. *Draconyx loureiroi* lacks the hypertrophied conical thumb (spike); instead, it possesses a series of claw-like unguals similar to those of *Camptosaurus dispar* and *Uteodon aphanocetes*. These data highlight the relationship between the close packing of the carpal bones and the presence of the hypertrophied pollex, although they raise the question from which ancestral condition the derived styracosternan carpus arose. The character state that resembles the possible ancestral condition most is the one present in *Camptosaurus dispar*, as the transition from a rigid interlocked unit to a fused element seems expected. In any case, *C. dispar* is recovered in a basal position with respect to the clade constituted of *D. loureiroi* and *U. aphanocetes*, indicating the immediate ancestral condition to the derived Early Cretaceous styracosternans is probably of these two latter forms (Fig. 14A–J). It is not clear if this result implies either re-evaluating *C. dispar* as a species or a deep revision of the characters present in our phylogenetic matrices, but both are beyond the scope of the present study.

The hindlimb elements show a mosaic of characters, found among several iguanodontian lineages. For instance, the preserved femoral shaft is strongly craniocaudally bowed, as it occurs in basal ornithopods, dryomorphans and ankylopollexians. Proximally, as in

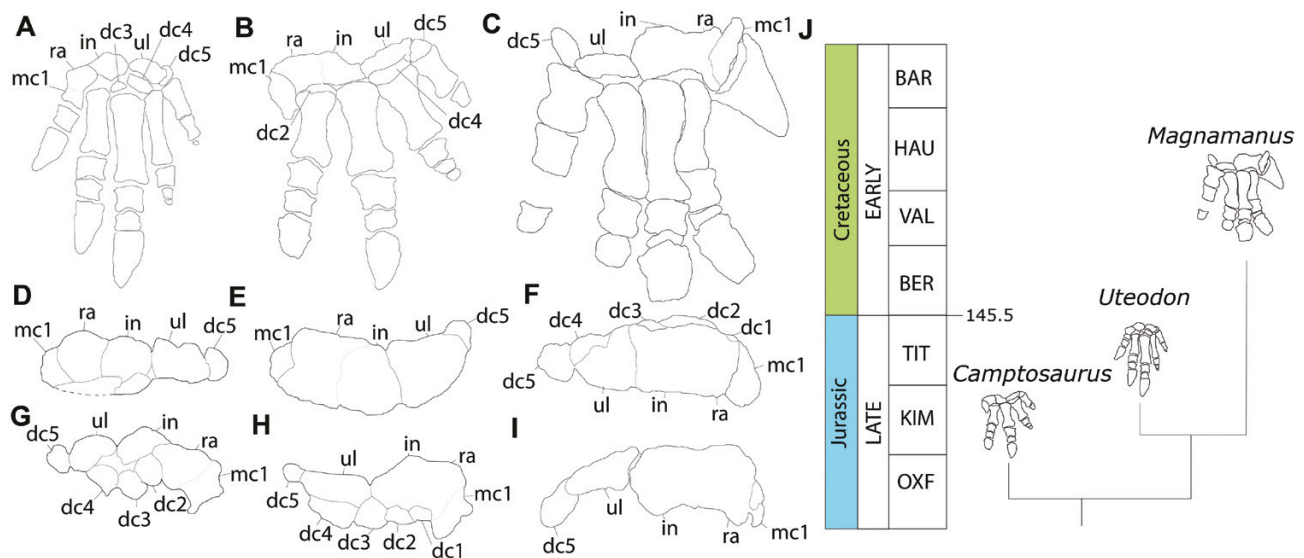


**Figure 14.** Comparison of the manual anatomy of selected styracosternans. *Uteodon aphanocetes* left manus (specimen CM 11337) in extensor view (A), proximal view (D) and palmar view (G). *Camptosaurus dispar* right manus, reversed (specimen USNM 4277) in extensor view (B), proximal view (E) and palmar view (H) (holotype USNM 4282). *Magnamanus soriaensis* right manus (holotype MNS 2000) in extensor view (C), proximal view (F) and palmar view (I). Note the difference in the structure of the carpus: *Uteodon aphanocetes* presents a partially fused and not closely packed carpus, *Camptosaurus dispar* presents a partially fused but closely packed carpus while *Magnamanus soriaensis* presents the typical stout and fused element of Styracosterna. J, Stratigraphic distribution of these characters. Abbreviations: dc1: distal carpal 1, dc2: distal carpal 2, dc3: distal carpal 3, dc4: distal carpal 4, dc5: distal carpal 5, in: intermedium, mc1: metacarpal 1, ra: radiale, ul: ulnare.

other ankylopollexian species (Gilmore, 1909; Norman, 1980, 1986, 2004), the femur may have a straighter outline, although the preservation bias hampers the possibility to properly assess this character. However, the mosaic of characters is most evident in the distal epiphysis: the extensor groove is deep and U-shaped as in *Valdosaurus canaliculatus* (Barrett *et al.*, 2011) and ankylopollexians basal to hadrosauriformes. The flexor groove is fully open, without the slight overhang that is found in some dryosaurid specimens (Galton, 1981), resembling the condition in basal ornithopod/ neornithischians (Fig. 7; Norman *et al.*, 2004).

Furthermore, the proximal epiphysis of the tibia has a concave medial margin in *Draconyx loureiroi*, as it occurs in elasmarians (Dieudonné *et al.*, 2021), while the fibular condyle is in an intermediate position between the one in basal ankylopollexians and derived ‘iguanodontoid’ taxa. In addition, as Dieudonné *et al.* (2021) noted in other Laurasian dryomorphans, the short cnemial crest is rounded and sharply defined and is strongly anterolaterally bowed, as is the one of other styracosternans (Norman, 1980, 1986, 2004). This plethora of characters needs further investigation, although it suggests the presence of a signal that may be related to geographical segregation or an adaptation in functional morphology.

*Draconyx loureiroi* has a gracile pes, compared with other ankylopollexians. The general proportions of metatarsals II–IV are similar to the lightly built species *Cumnoria prestwichii*, *Mantellisaurus atherfieldensis* and *Uteodon aphanoeectes*, and differing from the stout and robust condition found in *Camptosaurus dispar*, *Iguanodon bernissartensis* and other large-sized styracosternans (Galton & Powell, 1980; Norman, 1980, 1986; Carpenter & Wilson, 2008). Metatarsal I is present and extremely reduced, as in *Mantellisaurus atherfieldensis* and other derived styracosternans, and differing from dryosaurids and *Camptosaurus dispar*, which retain a larger and functional Mt I (Gilmore, 1909; Norman, 1980, 1986; Galton, 1981; Norman *et al.*, 2004).

Mateus & Antunes (2001) included *Draconyx loureiroi* in the clade ‘Camptosauridae’, then composed of the species *Camptosaurus depressus*, *C. dispar* and *C. prestwichii*. Carpenter & Wilson (2008) instituted the species *Camptosaurus aphanoeectes*, based on the specimens housed in the Carnegie Museum recovered from the Dinosaur National Monument, Utah. Subsequently, McDonald (2011) showed that the genus *Camptosaurus* is paraphyletic, including a set of progressively more deeply nested species, and recognized the following species as valid: *Camptosaurus dispar*, *Cumnoria prestwichii*, *Osmakasaurus depressus* and *Uteodon aphanoeectes*. However, Carpenter & Lamanna (2015) claimed that *Uteodon aphanoeectes* was based on a chimera and

placed the above-mentioned species back into the genus *Camptosaurus*.

At the present time, the monophyly of *Camptosaurus* and the clade ‘Camptosauridae’, as considered by Carpenter & Lamanna (2015), is not supported by phylogenetic analyses (i.e. McDonald, 2011; Verdú *et al.*, 2018), including the one presented in this study. Since specimens traditionally assigned to *Camptosaurus* sp. have been recovered from different stratigraphic intervals, anagenetic processes, such as the ones observed in the Dinosaur Park Formation (Mallon *et al.*, 2012; Carr *et al.*, 2017; Wilson *et al.*, 2020), might have led to the gradual acquisition of a mosaic of apomorphic and plesiomorphic character states. Until there has been a new assessment of the evolutionary history of iguanodontians in the Morrison Formation, we suggest that it is better to refer to the genus *Camptosaurus* as including just the species *C. dispar*.

#### TEMPO AND MODO OF BASAL IGUANODONTIAN DINOSAUR EVOLUTION

Two different methodologies indicate an increase of evolutionary rates at two geological moments: the first increase encompasses the Jurassic–Cretaceous transition, which is related to the origin of several styracosternan lineages and the second increase at around 80 Mya related to the origin of Rhabdodontidae and derived hadrosauroids. Benson *et al.* (2014, 2018) and Stubbs *et al.* (2019) found concordant trends with the ones recovered here. In particular, Benson *et al.* (2014, 2018) in their analyses of body-size evolution through time within Dinosauria located shifts in evolutionary rates of ornithopods in the Late Jurassic and Early Cretaceous at the base of Ankylopollexia and in the Late Cretaceous at the base of Rhabdodontidae and within the ‘eu-hadrosaurian’ lineage. Further, Benson *et al.* (2018) stated that ‘shifts to larger body size are more frequent than to smaller size in ornithischians’ with the evolutionary models that best describe the overall body-size evolution in dinosaurs as those of Ornstein-Uhlenbeck. These models describe constrained evolution around macro-evolutionary optima with rare rapid shifts towards different optima (Stanley, 1973; Hansen, 2013). Similarly, Stubbs *et al.* (2019) indicated a shift of evolutionary rates and a complex morphospace occupation in Hadrosauroidea.

The first shift in evolutionary rates is the most relevant in terms of its implications for the present contribution. Styracosterna is characterized by generally increased body size in comparison with basal iguanodontians (Norman, 2004). The appearance of some evolutionary novelties within this clade (i.e. straight femoral shaft, migration of the fourth trochanter towards the femoral midshaft,

partially enclosed extensor and flexor grooves, and hoof-like manual unguals) are related to this trend (Maidment & Barrett, 2012). Therefore, we consider the shifts recovered by these analyses as the same general trend and concordant with Ornstein-Uhlenbeck models of evolution as proposed by Benson *et al.* (2014, 2018). However, we recognize that several lineage-specific transformations may have occurred and diverged by this theoretical general trend, such as lineages at the base of Styracosterna, as discussed below. Although the findings presented here need further investigation, the convergence of our and previous analyses provides evidence for an interesting interplay of body-size and auto-ecological character variations in the radiation of iguanodontian dinosaurs. We hypothesize here that novel characters related to feeding and food processing may have opened the possibility of occupying new ecological niches for iguanodontians, which resulted, consequently, in an increase of body size, as indicated by Benson *et al.* (2018). This shift resulted in accelerated morphological innovations, producing several adaptations in the skeleton to sustain a semi-quadrupedal stance.

Indicating the ecological and geological drivers of the *tempo* and *modo* that led to this shift and the following diversity of styracosternans is difficult, since the Jurassic–Cretaceous transition is complex and characterized by various geological events, which led to faunal turnovers in marine and terrestrial ecosystems (Tennant *et al.*, 2017). The work by Tennant *et al.* (2016, 2017) proposed tectonic activity and eustatic

variation across the Jurassic–Cretaceous transition as the primary factors of diversity variation among several tetrapod groups, and this may have influenced the evolutionary rates of those clades passing through this transition.

#### IMPLICATIONS FOR THE RISE OF STYRACOSTERNA

Definitive styracosternans appeared no later than the Late Jurassic. The stratigraphic position of ML 357, close to the Kimmeridgian–Tithonian boundary, makes this specimen one of the oldest representatives of this group (Norman, 2004). *Cumnoria prestwichii* recovered by McDonald (2011) as a styracosternan is Late Kimmeridgian in age according to Benton & Spencer (1995), while *Uteodon aphanoecetes* is from the Lower–Middle Tithonian beds of the Brushy Basin Member of the Morrison Formation, being slightly younger than the above-mentioned species (Carpenter & Wilson, 2008). Therefore, *Cumnoria prestwichii* and *Draconyx loureiroi* should closely resemble the basal bauplan of Styracosterna. These two species share a lightly built skeleton, and gracile and elongate pedal morphology (Galton & Powell, 1980). The small size of *Draconyx loureiroi* is comparable with *Cumnoria prestwichii*, indicating that styracosternans were medium-sized animals, smaller than *Camptosaurus dispar* (Carpenter & Galton, 2018). Furthermore, the unfused and non-interlocked carpal and manual ungual condition of *Draconyx loureiroi* suggests a different locomotion



**Figure 15.** Life restoration of *Draconyx loureiroi*, in the environment represented by Lourinhã Formation. Credit: Victor Carvalho, used with permission under CC BY NC 4.0 license.

stance with respect to *Camptosaurus dispar*, which is considered primarily quadrupedal.

Maidment & Barrett (2012) have supported the interpretation that hoof-like manual unguals are strongly associated with a quadrupedal stance, as proposed by Galton (1970) and Norman (1986). Therefore, the lack of the above-mentioned characters strongly supports the interpretation of *Draconyx loureiroi* as a bipedal, possibly cursorial, animal inhabiting the forests of the Lourinhã Formation, as indicated by our restoration (Fig. 15). We propose the hypothesis that Styrcosterna arose as a group of relatively small, cursorial animals, which after the Late Jurassic radiated into larger forms, resulting from accelerated rates of evolution. Since the oldest representatives appear to be European, it is suggested that this clade originated in Europe and eventually dispersed globally. The *tempo* and *modo* of this radiation need to be better understood, integrating more data points, such as palaeogeography. We have also reinforced the hypothesis that derived iguanodontians appeared in Europe earlier than previously thought (Castanera *et al.*, 2020, 2021; Rotatori *et al.*, 2020).

## CONCLUSIONS

The ornithopod dinosaur *Draconyx loureiroi* is re-described and re-diagnosed, with new forelimb elements described for the first time. The holotype and only specimen is ML 357 and the previously referred material ML 434 is re-assigned to *Ankylopollexia indet.* Phylogenetic analysis and anatomical comparisons indicate that *Draconyx loureiroi* can be assigned to Styrcosterna. A unique combination of characters unambiguously distinguishes *D. loureiroi* from other species within the clade. The inclusion of *Draconyx loureiroi* within Styrcosterna makes it one of the oldest species that can be referred to this clade, suggesting a European origin for Styrcosterna and from which it later dispersed. The relatively small size of *D. loureiroi*, considered as a senile individual, suggests basal styrcosternans were bipedal and possibly cursorial animals, attaining larger body sizes and adaptations to quadrupedalism later in their evolution. Analyses of evolutionary rates, employing both maximum parsimony and Bayesian inference, reveal an increase of evolutionary rates among basal iguanodontians across the Jurassic–Cretaceous transition, as observed in other tetrapod clades.

## ACKNOWLEDGEMENTS

We thank Carlos Anunciação for making available unpublished and unreported material of the holotype

specimen of *Draconyx loureiroi*. We would like to thank Carla Tomás, Micael Martinho and Laura de Jorge for their help with preparation and lab assistance. We also thank all the technical staff of Museu da Lourinhã for access to facilities and assistance, especially Bruno Pereira and Alexandre Audigane. We thank the DinoParque Lourinhã and Simão Mateus for help with accessing the material, Dr Nuno Leal (Hospital Veterinário do Oeste) and the Miconsense Company for help and assistance with CT-SCAN, Victor Beccari for help with BLENDER software, Dr Andrea Cau for help and discussion on Bayesian inference, and Bruno Camilo Silva of Sociedade de História Natural for providing access to comparative material. We thank Dr Paul M. Barrett, Joseph Bonsor and an anonymous reviewer for their comments, which greatly improved this manuscript. We also thank Vincent J. Cheng for proof-reading an earlier version of this manuscript.

## FUNDING

Funding was provided by GeoBioTec grants, GeoBioTec-GeoBioSciences, GeoTechnologies and GeoEngineering NOVA [GeoBioCiências, GeoTecnologias e GeoEngenharias], grant UIDB/04035/2020 by the Fundação para a Ciência e Tecnologia and by the project BioGeoSauria, grant number: PTDC/CTA-PAL/2217/2021 supported by Fundação para a Ciência e a Tecnologia, Portugal. FMR is supported by the FCT grant SFRH/BD/146230/2019, and the research herein presented was funded by the Horácio Mateus Grant: DragonClaw, reappraisal of the holotype of *Draconyx loureiroi* from the Museu da Lourinhã. MMA is supported by Fundação para a Ciência e Tecnologia, Grant Number SFRH/BPD/113130/2015.

## DATA AVAILABILITY

All available data available is given in the supporting information of this paper.

## REFERENCES

- Baron MG. 2019. *Pisanosaurus mertii* and the Triassic ornithischian crisis: could phylogeny offer a solution? *Historical Biology* **31**: 967–981.
- Barrett PM. 2016. A new specimen of *Valdosaurus canaliculatus* (Ornithopoda: Dryosauridae) from the Lower Cretaceous of the Isle of Wight, England. *Memoirs of Museum Victoria* **74**: 29–48.
- Barrett PM, Butler RJ, Twitchett RJ, Hutt S. 2011. New material of *Valdosaurus canaliculatus* (Ornithischia: Ornithopoda) from the Lower Cretaceous of southern England. *Special Papers in Palaeontology* **86**: 131–163.

- Becerra MG, Ramírez MA. 2018.** Locomotor morphotypes, allometry, linear regressions and the smallest sizes in Ornithischia: estimating body length using hind limb variables. *Ameghiniana* **55**: 491–516.
- Bell PR, Herne MC, Brougham T, Smith ET. 2018.** Ornithopod diversity in the Griman Creek Formation (Cenomanian), New South Wales, Australia. *PeerJ* **6**: e6008.
- Benson RB, Campione NE, Carrano MT, Mannion PD, Sullivan C, Upchurch P, Evans DC. 2014.** Rates of dinosaur body mass evolution indicate 170 million years of sustained ecological innovation on the avian stem lineage. *PLoS Biology* **12**: e1001853.
- Benson RB, Hunt G, Carrano MT, Campione N. 2018.** Cope's rule and the adaptive landscape of dinosaur body size evolution. *Palaeontology* **61**: 13–48.
- Benton MJ, Spencer PS. 1995.** British Late Jurassic fossil reptile sites. In: Benton MJ, Spencer PS, eds. *Fossil reptiles of Great Britain*. Dordrecht: Springer, 165–214.
- Bertozzo F, Dalla Vecchia FM, Fabbri M. 2017.** The Venice specimen of *Ouranosaurus nigeriensis* (Dinosauria, Ornithopoda). *PeerJ* **5**: e3403.
- Boyd CA. 2015.** The systematic relationships and biogeographic history of ornithischian dinosaurs. *PeerJ* **3**: e1523.
- Carpenter K, Galton PM. 2018.** A photo documentation of bipedal ornithischian dinosaurs from the Upper Jurassic Morrison Formation, USA. *Geology of the Intermountain West* **5**: 167–207.
- Carpenter K, Lamanna MC. 2015.** The braincase assigned to the ornithopod dinosaur *Uteodon* McDonald, 2011, reassigned to *Dryosaurus* Marsh, 1894: implications for iguanodontian morphology and taxonomy. *Annals of Carnegie Museum* **83**: 149–166.
- Carpenter K, Wilson Y. 2008.** A new species of *Camptosaurus* (Ornithopoda: Dinosauria) from the Morrison Formation (Upper Jurassic) of Dinosaur National Monument, Utah, and a biomechanical analysis of its forelimb. *Annals of Carnegie Museum* **76**: 227–264.
- Carr TD, Varricchio DJ, Sedlmayr JC, Roberts EM, Moore JR. 2017.** A new tyrannosaur with evidence for anagenesis and crocodile-like facial sensory system. *Scientific Reports* **7**: 44942.
- Castanera D, Silva BC, Santos VF, Malafaia E, Belvedere M. 2020.** Tracking Late Jurassic ornithopods in the Lusitanian Basin of Portugal: ichnotaxonomic implications. *Acta Palaeontologica Polonica* **65**: 399–412.
- Castanera D, Malafaia E, Silva BC, Santos VF, Belvedere M. 2021.** New dinosaur, crocodylomorph and swim tracks from the Late Jurassic of the Lusitanian Basin: implications for ichnodiversity. *Lethaia* **54**: 271–287.
- Dieudonné PE, Tortosa T, Torcida Fernández-Baldor F, Canudo JI, Díaz-Martínez I. 2016.** An unexpected early rhabdodontid from Europe (Lower Cretaceous of Salas de los Infantes, Burgos Province, Spain) and a re-examination of basal iguanodontian relationships. *PLoS One* **11**: e0156251.
- Dieudonné PE, Cruzado-Caballero P, Godefroit P, Tortosa T. 2021.** A new phylogeny of cerapodan dinosaurs. *Historical Biology* **33**: 2335–2355.
- Dodson P. 1980.** Comparative osteology of the American ornithopods *Camptosaurus* and *Tenontosaurus*. *Memoirs of the Society of Geology, France* **139**: 81–85.
- Escaso F. 2014.** *Historia evolutiva de los Ornithischia (Dinosauria) del Jurásico Superior de Portugal*. 300 pp. Doctoral Dissertation, Universidad Autónoma de Madrid, Madrid.
- Escaso F, Ortega F, Dantas P, Malafaia E, Silva BC, Gasulla JM, Mocho P, Narváez I, Sanz JL. 2014.** A new dryosaurid ornithopod (Dinosauria, Ornithischia) from the Late Jurassic of Portugal. *Journal of Vertebrate Paleontology* **34**: 1102–1112.
- Erickson BR. 1988.** *Notes on the postcranium of Camptosaurus*. St Paul: Scientific Publications of the Science Museum of Minnesota, 6–13.
- Forster CA. 1990.** The postcranial skeleton of the ornithopod dinosaur *Tenontosaurus tilletti*. *Journal of Vertebrate Paleontology* **10**: 273–294.
- Foster J. 2020.** *Jurassic West: the dinosaurs of the Morrison Formation and their world, 2nd edn*. Bloomington: Indiana University Press.
- Galton PM. 1970.** The posture of hadrosaurian dinosaurs. *Journal of Paleontology* **44**: 464–473.
- Galton PM. 1974.** *The ornithischian dinosaur Hypsilophodon from the Wealden of the Isle of Wight*. London: British Museum (Natural History).
- Galton PM. 1975.** English hypsilophodontid dinosaurs (Reptilia: Ornithischia). *Palaeontology* **18**: 741–752.
- Galton PM. 1980.** European Jurassic ornithopod dinosaurs of the families Hypsilophodontidae and Camptosauridae. *Neues Jahrbuch für Geologie und Paläontologie, Abhandlungen* **160**: 73–95.
- Galton PM. 1981.** *Dryosaurus*, a hypsilophodontid dinosaur from the Upper Jurassic of North America and Africa postcranial skeleton. *Paläontologische Zeitschrift* **55**: 271–312.
- Galton PM. 1983.** The cranial anatomy of *Dryosaurus*, a hypsilophodontid dinosaur from the Upper Jurassic of North America and East Africa, with a review of hypsilophodontids from the Upper Jurassic of North America. *Geologica et Palaeontologica* **17**: 207–243.
- Galton PM. 2006.** *Teeth of ornithischian dinosaurs (mostly Ornithopoda) from the Morrison Formation (Upper Jurassic) of western United States. Horns and beaks. Ceratopsian and Ornithopod dinosaurs*. Bloomington: Indiana University Press, 17–47.
- Galton PM. 2009.** Notes on Neocomian (Lower Cretaceous) ornithopod dinosaurs from England – *Hypsilophodon*, *Valdosaurus*, '*Camptosaurus*', '*Iguanodon*' – and referred specimens from Romania and elsewhere. *Revue de Paléobiologie* **28**: 211–273.
- Galton PM, Powell HP. 1980.** The ornithischian dinosaur *Camptosaurus prestwichii* from the Upper Jurassic of England. *Palaeontology* **23**: 411–443.
- Gilmore CW. 1909.** Osteology of the Jurassic reptile *Camptosaurus*: with a revision of the species of the genus, and description of two new species. *Proceedings of the United States National Museum* **36**: 197–332.

- Goloboff PA, Catalano SA. 2016.** TNT v.1.5, including a full implementation of phylogenetic morphometrics. *Cladistics* **32**: 221–238.
- Hansen TF. 2013.** Adaptive landscapes and macroevolutionary dynamics. In: Svensson E, Calsbeek R, eds. *The adaptive landscape in evolutionary biology*. Oxford: Oxford University Press, 205–226.
- Heath TA, Huelsenbeck JP, Stadler T. 2014.** The fossilized birth–death process for coherent calibration of divergence-time estimates. *Proceedings of the National Academy of Sciences of the USA* **111**: E2957–E2966.
- Herne MC, Tait AM, Weisbecker V, Hall M, Nair JP, Cleeland M, Salisbury SW. 2018.** A new small-bodied ornithopod (Dinosauria, Ornithischia) from a deep, high-energy Early Cretaceous river of the Australian–Antarctic rift system. *PeerJ* **5**: e4113.
- Herne MC, Nair JP, Evans AR, Tait AM. 2019.** New small-bodied ornithopods (Dinosauria, Neornithischia) from the Early Cretaceous Wonthaggi Formation (Strzelecki Group) of the Australian–Antarctic rift system, with revision of *Qantassaurus intrepidus* Rich and Vickers-Rich, 1999. *Journal of Paleontology* **93**: 1–42.
- Hess R. 2010.** *Blender foundations: the essential guide to learning Blender 2.6*. Waltham: Focal Press.
- Hill G. 1889.** Distal alluvial fan sediments from the Upper Jurassic of Portugal: controls on their cyclicity and channel formation. *Journal of the Geological Society* **146**: 539–555.
- Hulke JW. 1880.** *Iguanodon prestwichii*, a new species from the Kimmeridge Clay, founded on numerous fossil remains lately discovered at Cumnor, near Oxford. *Quarterly Journal of the Geological Society* **36**: 433–456.
- Ibircu LM, Casal GA, Martínez RD, Luna M, Canale JI, Álvarez BN, González Riga B. 2019.** A new ornithopod dinosaur (Dinosauria: Ornithischia) from the Late Cretaceous of central Patagonia. *Cretaceous Research* **98**: 276–291.
- Kullberg JC, da Rocha RB, Soares AF, Duarte LV, Marques JF. 2014.** Palaeogeographical evolution of the Lusitanian Basin (Portugal) during the Jurassic. Part I: the tectonic constraints and sedimentary response. In: da Rocha RB, Pais J, Kullberg JC, Finney S, eds. *STRATI 2013*. Cham: Springer, 665–672.
- Lewis PO. 2001.** A likelihood approach to estimating phylogeny from discrete morphological character data. *Systematic Biology* **50**: 913–925.
- Lydekker R. 1888a.** Note on a new Wealden iguanodont and other dinosaurs. *Quarterly Journal of the Geological Society of London* **44**: 46–61.
- Madzia D, Boyd CA, Mazuch M. 2018.** A basal ornithopod dinosaur from the Cenomanian of the Czech Republic. *Journal of Systematic Palaeontology* **16**: 967–979.
- Maidment SC, Barrett PM. 2012.** Osteological correlates for quadrupedality in ornithischian dinosaurs. *Acta Palaeontologica Polonica* **59**: 53–70.
- Mallon JC, Evans DC, Ryan MJ, Anderson JS. 2012.** Megaherbivorous dinosaur turnover in the Dinosaur Park Formation (upper Campanian) of Alberta, Canada. *Palaeogeography, Palaeoclimatology, Palaeoecology* **350**: 124–138.
- Mantell GA. 1825.** Notice on the *Iguanodon*, a newly discovered fossil reptile, from the sandstone of Tilgate Forest, in Sussex. *Philosophical Transactions of the Royal Society of London* **115**: 179–186.
- Marsh OC. 1878.** Principal characters of American Jurassic dinosaurs. Part I. *American Journal of Science and Arts* **16**: 411–416.
- Marsh OC. 1879.** Notice of new Jurassic reptiles. *American Journal of Science and Arts* **18**: 501–506.
- Marsh OC. 1881.** Principal characters of American Jurassic dinosaurs. Part V. *American Journal of Science (Series 3)* **21**: 417–423.
- Mateus O, Antunes MT. 2001.** *Draconyx loureiroi*, a new camptosauridae (Dinosauria, Ornithopoda) from the Late Jurassic of Lourinhã, Portugal. *Annales de Paléontologie* **87**: 61–73.
- Mateus O, Dinis J, Cunha PP. 2017.** The Lourinhã Formation: the upper Jurassic to lowermost Cretaceous of the Lusitanian Basin, Portugal – landscapes where dinosaurs walked. *Ciências Da Terra – Earth Sciences Journal* **19**: 75–97.
- McDonald AT. 2011.** The taxonomy of species assigned to *Camptosaurus* (Dinosauria: Ornithopoda). *Zootaxa* **2783**: 52–68.
- McDonald AT. 2012.** Phylogeny of basal iguanodonts (Dinosauria: Ornithischia): an update. *PLoS One* **7**: e36745.
- McDonald AT, Kirkland JI, DeBlieux DD, Madsen SK, Cavin J, Milner AR, Panzarin L. 2010b.** New basal iguanodonts from the Cedar Mountain Formation of Utah and the evolution of thumb-spiked dinosaurs. *PLoS One* **5**: e14075.
- McDonald AT, Espílez E, Mampel L, Kirkland JI, Alcalá L. 2012.** An unusual new basal iguanodont (Dinosauria: Ornithopoda) from the Lower Cretaceous of Teruel, Spain. *Zootaxa* **3595**: 61–76.
- Milner AR, Norman DB. 1984.** The biogeography of advanced ornithopod dinosaurs (Archosauria: Ornithischia) – a cladistic-vicariance model. In: Reif E, Westphal F, eds. *Third Symposium on Mesozoic Terrestrial Ecosystems, Short Papers*, 145–150. Tübingen: Attempto Verlag.
- Norman DB. 1980.** On the ornithischian dinosaur *Iguanodon bernissartensis* from the lower Lower Cretaceous of Bernissart (Belgium). *Memoir de l’Institut Royal des Sciences Naturelles de Belgique* **178**: 1–105.
- Norman DB. 1986.** On the anatomy of *Iguanodon atherfieldensis* (Ornithischia: Ornithopoda). *Bulletin de l’Institut Royal des Sciences Naturelles de Belgique* **56**: 281–372.
- Norman DB. 2004.** Basal iguanodontia. In: Weishampel DB, Dodson P, Osmolska H, eds. *The Dinosauria*. Berkeley: University of California, 413–437.
- Norman DB. 2011.** On the osteology of the lower Wealden (Valanginian) ornithopod *Barilium dawsoni* (Iguanodontia: Styracosterna). *Special Papers in Palaeontology* **86**: 165–194.
- Norman DB. 2015.** On the history, osteology, and systematic position of the Wealden (Hastings group) dinosaur *Hypselospinus fittoni* (Iguanodontia: Styracosterna). *Zoological Journal of the Linnean Society* **173**: 92–189.

- Norman DB, Sues HD, Witmer LM, Coria RA. 2004.** Basal ornithopoda. In: Weishampel DB, Dodson P, Osmolska H, eds. *The Dinosauria*. Berkeley: University of California, 393–412.
- Novas F, Cambiaso A, Ambrosio A. 2004.** A new basal iguanodontian (Dinosauria, Ornithischia) from the Upper Cretaceous of Patagonia. *Ameghiniana* **41**: 75–82.
- Owen R. 1842.** Report on British fossil reptiles. Part II. In: *Report of the eleventh meeting of the British association for the advancement of science, Plymouth, England, July 1841*. London: John Murray, 60–204.
- Pol D, Escapa IH. 2009.** Unstable taxa in cladistic analysis: identification and the assessment of relevant characters. *Cladistics* **25**: 515–527.
- Rambaut A, Drummond AJ, Xie D, Baele G, Suchard MA. 2018.** Posterior summarization in Bayesian phylogenetics using Tracer 1.7. *Systematic Biology* **67**: 901–904.
- Rauhut OW, Pol D. 2019.** Probable basal allosauroid from the early Middle Jurassic Cañadón Asfalto Formation of Argentina highlights phylogenetic uncertainty in tetanuran theropod dinosaurs. *Scientific Reports* **9**: 1–9.
- Ronquist F, Teslenko M, van der Mark P, Ayres DL, Darling A, Höhna S, Larget B, Liu L, Suchard MA, Huelsenbeck JP. 2012.** MrBayes 3.2: efficient Bayesian phylogenetic inference and model choice across a large model space. *Systematic Biology* **61**: 539–542.
- Rotatori FM, Moreno-Azanza M, Mateus O. 2020.** New information on ornithopod dinosaurs from the Late Jurassic of Portugal. *Acta Palaeontologica Polonica* **65**: 35–57.
- Rozadilla S, Agnolín FL, Novas FE. 2019.** Osteology of the Patagonian ornithopod *Talenkauen santacruzensis* (Dinosauria, Ornithischia). *Journal of Systematic Palaeontology* **17**: 2043–2089.
- Rozadilla S, Cruzado-Caballero P, Calvo JO. 2020.** Osteology of Ornithopod *Macrogyphosaurus gondwanicus* (Dinosauria, Ornithischia) from the Upper Cretaceous of Patagonia, Argentina. *Cretaceous Research* **108**: 104311.
- Ruiz-Omeñaca JI, Pereda Suberbiola X, Galton PM. 2006.** *Callovosaurus leedsi*, the earliest dryosaurid dinosaur (Ornithischia: Euornithopoda) from the Middle Jurassic of England. In: Carpenter K, ed. *Horns and beaks: ceratopsian and ornithopod dinosaurs*. Bloomington: Indiana University Press, 3–16.
- Seeley HG. 1887.** On the classification of the fossil animals commonly called Dinosauria. *Proceedings of the Royal Society of London* **43**: 165–17.
- Sereno PC. 1986.** Phylogeny of the bird-hipped dinosaurs (order Ornithischia). *National Geographic Research* **2**: 234–256.
- Simões TR, Vernygora O, Caldwell MW, Pierce SE. 2020a.** Megaevolutionary dynamics and the timing of evolutionary innovation in reptiles. *Nature Communications* **11**: 1–14.
- Simões TR, Caldwell MW, Pierce SE. 2020b.** Sphenodontian phylogeny and the impact of model choice in Bayesian morphological clock estimates of divergence times and evolutionary rates. *BMC Biology* **18**: 1–30.
- Stanley SM. 1973.** An explanation for Cope's rule. *Evolution* **27**: 1–26.
- Stubbs TL, Benton MJ, Elsler A, Prieto-Márquez A. 2019.** Morphological innovation and the evolution of hadrosaurid dinosaurs. *Paleobiology* **45**: 347–362.
- Tennant JP, Mannion PD, Upchurch P. 2016.** Sea level regulated tetrapod diversity dynamics through the Jurassic/Cretaceous interval. *Nature Communications* **7**: 1–11.
- Tennant JP, Mannion PD, Upchurch P, Sutton MD, Price GD. 2017.** Biotic and environmental dynamics through the Late Jurassic–Early Cretaceous transition: evidence for protracted faunal and ecological turnover. *Biological Reviews* **92**: 776–814.
- Taquet P. 1976.** *Géologie et paléontologie du Gisement de Gadoufaoua (Aptien du Niger)*. Paris: Editions du Centre National de la Recherche Scientifique.
- Taylor AM, Gowland S, Leary S, Keogh KJ, Martinus AW. 2014.** Stratigraphical correlation of the Late Jurassic Lourinhã Formation in the Consolação Sub-basin (Lusitanian Basin), Portugal. *Geological Journal* **49**: 143–162.
- Van Beneden PJ. 1881.** Sur l'arc pelvien chez les dinosauriens de Bernissart (review of G. A. Boulenger). *Bulletin de l'Académie Royale des Sciences, des Lettres et des Beaux-Arts de Belgique (3rd ser.)* **1**: 600–608.
- Verdú FJ, Royo-Torres R, Cobos A, Alcalá L. 2018.** New systematic and phylogenetic data about the early Barremian *Iguanodon galvensis* (Ornithopoda: Iguanodontoidea) from Spain. *Historical Biology* **30**: 437–474.
- Verdú FJ, Cobos A, Royo-Torres R, Alcalá L. 2019.** Diversity of large ornithopod dinosaurs in the upper Hauterivian–lower Barremian (Lower Cretaceous) of Teruel (Spain): a morphometric approach. *Spanish Journal of Palaeontology* **34**: 269–288.
- Vidarte CF, Calvo MM, Fuentes FM, Fuentes MM. 2016.** Un nuevo dinosaurio estiracosterno (Ornithopoda: Ankylopollexia) del Cretácico Inferior de España. *Spanish Journal of Palaeontology* **31**: 407–446.
- Virchow H. 1919.** Atlas und Epistropheus bei den Schildkröten. *Sitzungsberichte der Gesellschaft Naturforschender Freunde zu Berlin* **8**: 303–332.
- Waskow K, Mateus O. 2017.** Dorsal rib histology of dinosaurs and a crocodylomorph from western Portugal: skeletochronological implications on age determination and life history traits. *Comptes Rendus Palevol* **16**: 425–439.
- Weishampel DB, Bjork PR. 1989.** The first indisputable remains of *Iguanodon* (Ornithischia: Ornithopoda) from North America: *Iguanodon lakotaensis*, sp. nov. *Journal of Vertebrate Paleontology* **9**: 56–66.
- Wilson JP, Ryan MJ, Evans DC. 2020.** A new, transitional centrosaurine ceratopsid from the upper cretaceous two medicine formation of Montana and the evolution of the 'Styracosaurus-line' dinosaurs. *Royal Society Open Science* **7**: 200284.
- Winkler DA, Murry PA, Jacobs LL. 1997.** A new species of *Tenontosaurus* (Dinosauria: Ornithopoda) from the Early Cretaceous of Texas. *Journal of Vertebrate Paleontology* **17**: 330–348.
- Xu X, Tan Q, Gao Y, Bao Z, Yin Z, Guo B, Wang J, Tan L, Zhang Y, Xing H. 2018.** A large-sized basal ankylopollexian from East Asia, shedding light on early biogeographic history of Iguanodontia. *Science Bulletin* **63**: 556–563.

### SUPPORTING INFORMATION

Additional Supporting Information may be found in the online version of this article at the publisher's web-site.

**File S1.** Data matrix of [Madzia \*et al.\* \(2018\)](#) implementing [Bell \*et al.\*'s \(2018\)](#) modifications, including ML 357.

**File S2.** Data matrix of [Xu \*et al.\* \(2018\)](#) including ML 357.

**File S3.** Nexus infile of the non-clock analysis.

**File S4.** Nexus infile of the clock analysis.

**File S5.** 3D file of the articulated leg of *Draconyx loureiroi* holotype, ML 357.